AD-A080 617 DEFENCE RESEARCH ESTABLISHMENT ATLANTIC DARTMOUTH (NO--ETC F/G 20/4
WATER TUNNEL TESTS ON A NACA 16-309 SECTION EQUIPPED WITH A SIM--ETC(U)
DEC 79 E A JONES, M MACKAY
UNCLASSIFIED DREA-TM-79/C NL

| OF |
AD
A080617

END
DATE
FILMED
3 - 80
DDC

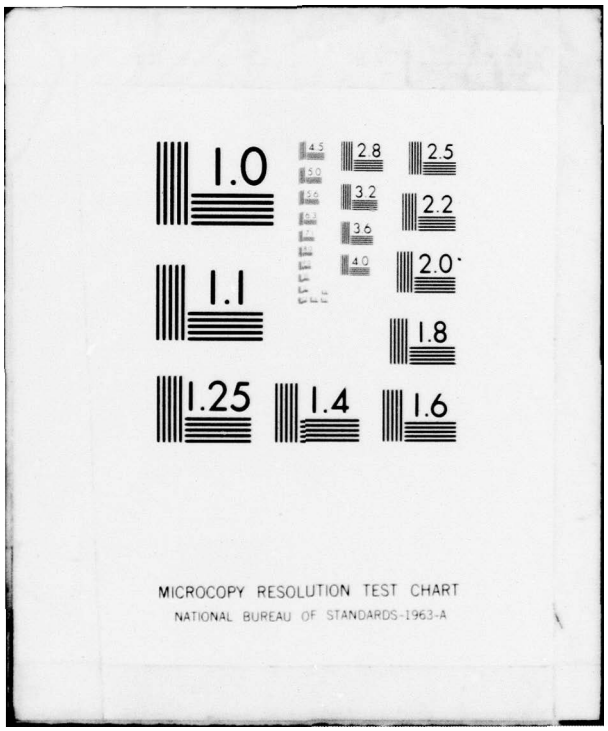
1.0
1.1
1.25
1.4
1.6
1.8
2.0
2.2
2.5
2.8
3.2
3.6
4.0
4.5
5.0
5.6
6.3
7.1
MICROCOPY RESOLUTION TEST CHART
NATIONAL BUREAU OF STANDARDS-1963-A

DEFENCE RESEARCH ESTABLISHMENT
ATLANTIC

3

LEVEL II





# WATER TUNNEL TESTS ON A NACA 16-309 SECTION EQUIPPED WITH A SIMPLE, SEALED FLAP

D.R.E.A. TECHNICAL MEMORANDUM 79/C

RESEARCH AND DEVELOPMENT BRANCH
DEPARTMENT OF NATIONAL DEFENCE
CANADA

(2)

DEFENCE RESEARCH ESTABLISHMENT
ATLANTIC

DARTMOUTH N.S.

D. R. E. A. TECHNICAL MEMORANDUM 79/C

(9) (3)

(14) DREA-TM-79/C

(6) WATER TUNNEL TESTS ON A NACA 16-309 SECTION EQUIPPED WITH A SIMPLE, SEALED FLAP.

(10) Eric A. JONES Michael MACKAY

(11) DEC[redacted]79

(12) 63



Approved by J.R. BROWN A/Director / Technology Division

DISTRIBUTION APPROVED BY

CHIEF D. R. E. A.

RESEARCH AND DEVELOPMENT BRANCH
DEPARTMENT OF NATIONAL DEFENCE
CANADA

403 761

## ABSTRACT

Water tunnel tests are described of a NACA 16-309 section equipped with a 25% flap-chord ratio, simple, sealed flap. Lift and pitching moment coefficients are given for a range of angles of attack, flap angles and cavitation numbers. Drag data are not considered reliable and only a few values are presented. The results are also given of limited tests for the dependency of force, moment and cavitation inception data on Reynolds number over the range from 1.25 to 3.98 x $10^6$.

## SOMMAIRE

On décrit les essais qu'on a fait subir en galerie hydraulique à une section du profil aérodynamique NACA 16-309 munie d'un volet hypersustentateur étanche simple ayant un rapport volet/corde de profil de 25%. On présente les coefficients de portance et du moment de tangage pour une gamme d'angles d'attaque, d'angles d'inclinaison du volet et de nombres de cavitation. On estime que les données relatives à la traînée ne sont pas fiables et on n'en donne que quelques valeurs. On présente également les résultats d'essais limités ayant trait à la dépendance de la force de sustentation, du moment et de la cavitation sur une gamme de nombres Reynolds allant de 1.25 à 3.98 x $10^6$.

TABLE OF CONTENTS

## NOMENCLATURE

| | |
|---|---|
| $C_d$ | section drag coefficient |
| $C_\ell$ | section lift coefficient |
| $C_{\ell\alpha}$ | rate of change of lift coefficient with angle of attack (degrees$^{-1}$) |
| $C_{\ell\delta}$ | rate of change of lift coefficient with flap angle (degrees$^{-1}$) |
| $C_m$ | section quarter chord pitching moment coefficient |
| $C_{m\delta}$ | rate of change of pitching moment with flap angle (degrees$^{-1}$) |
| Re | Reynolds number |
| $\alpha$ | angle of attack (degrees) |
| $\delta$ | flap angle (degrees) |
| $\sigma$ | cavitation number |
| f | flap chord ratio |
| $x_c$ | abscissa of point on section surface |
| $y_u$ | ordinate of point on section upper surface |
| $y_\ell$ | ordinate of point on section lower surface |

# 1. INTRODUCTION

The NACA 16 Series of airfoil sections was designed originally for high speed airfoil applications, where a uniform distribution of pressure is desired on the upper surface at design lift coefficient. This condition also gives favourable cavitation characteristics, a factor of great importance in hydrofoil section design since cavitation sets practical limits to the maximum speed, take-off speed and degree of control which can be obtained. Consequently, the section has found considerable use in fully-submerged hydrofoils, both with incidence control and with a simple, sealed flap for control purposes.

Results were published in 1948 of wind tunnel tests on a series of Type 16 sections[1], covering a fairly wide range of lift coefficients and thickness-to-chord ratios, but no data were available giving the basic characteristics of the section equipped with a control flap for hydrofoil use. Such data are desirable for hydrofoil ship design and performance predictions and can provide a valuable check on the accuracy of prediction techniques being developed for the analysis of flow over flapped hydrofoils. They can also be expected to provide a standard for comparison with new hydrofoil sections developed to take advantage of improved analytical techniques.

To meet the requirement for basic data, a program of tests was undertaken on a NACA 16-309 section with an $a = 1.0$ mean camber line and with a 25% flap-chord ratio, simple, sealed flap. This particular section was selected because it is fitted on USS "HIGHPOINT" (PCH-1), a 128 ton auw hydrofoil ship used extensively by DTNSRDC for hydrofoil research. It consequently presents the best opportunity for comparison with three-dimensional model tests and with full scale operation.

The section test program included both water tunnel and wind tunnel tests. The primary objective of water tunnel tests, carried out at the California Institute of Technology (CIT), was to determine the cavitation characteristics for a range of flap angles and angles of attack, and their effects on the lift, drag and pitching moment characteristics. The wind tunnel tests were made to obtain more accurate force and moment data and also to obtain the pressure distribution characteristics, since these are obtained much more readily in the wind tunnel.

The purpose of this report is to present and analyze the data from the water tunnel tests. The model, experimental facility, instrumentation and test procedure are described in some detail. A fairly extensive analysis of the experimental data is then presented, from which a number of significant conclusions are drawn. For completeness, the test data plots are given in full in Appendix A.

A consideration of fundamental importance in any model test program is the influence of scale effects. Recent work[2,3] indicates that cavitation inception is not simply dependent on the local static pressure. It can originate as a result of fairly large pressure fluctuations associated with transition from laminar to turbulent flow. The location of the transition point along the length of the chord is Reynolds number dependent and thus, the inception of cavitation can also be Reynolds number dependent. The CIT tests were made mostly at a tunnel water speed of 50 ft/sec, giving a chord Reynolds number of $2.49 \times 10^6$. The highest Reynolds number possible was $3.98 \times 10^6$ which, although high by model test standards, is still significantly smaller than the representative value for USS HIGHPOINT of $2.5 \times 10^7$. Tests were therefore made to investigate the sensitivity of cavitation occurrence to Reynolds number over the available range. Reynolds number sensitivity tests were also made on the force and moment data.

The wind tunnel test series[4], which was run on a similar model of 30 inches chord at Reynolds numbers up to $4 \times 10^6$, provides further data on scale effects. Use is made of these data in discussing scale effects arising from different boundary layer flow characteristics.

## 2. MODEL DESCRIPTION

The six inch chord, six inch span water tunnel model was made from 17-4PH steel hardened to the H900 condition. It is shown in Figure 1, complete with tunnel wall fairing disc and ready for installation. The flap could be positioned at discrete angle settings of: -10°, -5°, 0°, 2.5°, 5°, 7.5°, 10°, 15° and 20°. The setting plate and the hole alignments used to obtain the required flap angles are illustrated in Figure 2 which shows the model with fairing disc removed. A separate securing plate was required at the free end of the model for each flap angle setting.

The section coordinates were derived from the standard data given by Abbott and Von Doenhoff[5], using a cubic spline fit

into a leading edge radius of 0.024 inch. The coordinates are given in Table I. Profile measurements were made on the completed model by CIT, along the axes shown in Figure 3. Measurements along axes A, B and C indicate virtually no twist along the span. Deviations from the specified section profiles along D, E and F are illustrated in Figure 4. This shows the error-to-chord ratio to be generally less than 0.0005. In the vicinity of the hinge-line, there is a deviation in the surface contour which is higher and steeper than desirable. There is a second deviation at about 5% chord, not as large in amplitude but equally steep. The model finish was generally fine and polished. Castings of the leading edge, sectioned at mid-span, were inspected on an optical comparator at a magnification of 20X and revealed no roughness or discontinuity in the curvature. It is difficult to obtain very high profile accuracies in the small size of model required for water tunnel testing. These profile errors are considered to be within the normal range of expectation for a relatively complicated model incorporating a hinged flap.

## 3. FACILITY AND INSTRUMENTATION

The High Speed Water Tunnel in the Graduate Aeronautical Laboratories of the California Institute of Technology (GALCIT)[6] was used in the performance of this experiment. For these tests, the tunnel was equipped with the two-dimensional working section shown in Figure 5. Test section pressure and water velocity could be controlled independently over a wide range and gases released by cavitation on the model were reabsorbed before the flow reentered the working section.

The model was viewed through a four-inch thick "Plexiglas" window, the inside surface of which was parallel to the theoretical centerline of the tunnel. The opposite wall was adjustable and rigidly attached to the tunnel at the upstream end. The position of this wall was adjusted to compensate for the effects of longitudinal pressure gradient due to wall boundary layer growth. The model fairing plate was fitted flush with the wall and great care was taken to avoid spurious flow disturbances due to discontinuities.

The hydrofoil model was supported as a cantilever from a three-component strain gage balance equipped with interchangeable load cells. The highest ranges available were used for these tests. These were: lift $\pm$ 800 lbs, drag $\pm$ 200 lbs, pitching moment $\pm$ 1200 inch-lbs. Each of the three output signals was amplified, digitised and simultaneously time-averaged.

Signals were displayed on panel meters and recorded on punched cards.

Working section velocity was determined by measuring the static pressure difference between the settling chamber upstream of the nozzle and the entrance to the working section, using a mercury-water manometer. Manometer readings were converted to velocity through an experimentally-determined calibration factor, based on measurements made with a Prandtl type pitot-static tube. Working section pressure was measured by means of a mercury barometer connected to the piezometer row at the entrance to the working section and referenced to the horizontal centerline of the working section.

The axial turbulence level, measured on the centerline at the balance station was less than 0.25% and was estimated by CIT[6] to be 0.2%. The dissolved gas content was measured at between 12 and 14 parts per million.

## 4. PROCEDURE

The model was mounted with its chord line parallel to the centerline of the working section for an angle of attack of zero degrees. The working section wall was set to give a nearly zero horizontal pressure gradient over the range of water velocities.

At the start of the program, the conventional "Plexiglas" viewing window was used, with the gap between it and the free end of the model set to 0.030 inch. This gap was required to prevent interference as the window deflects under differential pressure when the working section pressure was reduced. For the later part of the program, the "Plexiglas" sidewall was replaced by a stronger, aluminum plate, 1.75 inches thick, with a small, 7.5 inch diameter viewing port. The tip gap was reduced to 0.020 inch for this installation. The type of window used is listed in Table II for the given test conditions. The aluminum plate was used for all Reynolds number dependence tests, where positive tank pressures were involved and, as a matter of convenience, for all tare runs. Measurements of window deflection as a function of working section pressure are presented in Figure 6.

Since the model had to be removed from the tunnel each time that the flap angle was adjusted, test series were run with fixed flap angle and with angle of attack, Reynolds or cavitation numbers as variables. For the Reynolds number

surveys, runs were made at fixed angle of attack and flap angle at speeds of 25, 40, 50, 70 and 80 ft/sec, giving chord Reynolds numbers of 1.25, 1.99, 2.49, 3.49 and 3.98 x $10^6$ respectively. Tunnel pressures were increased or decreased as required to obtain cavitation-free running and to measure the cavitation numbers for inception and desinence at the leading edge and hinge-line. The corresponding balance measurements were then recorded.

For the cavitation survey, runs were made at a constant water speed of 50 ft/sec, a compromise speed which allowed reasonable ranges of flap angle and angle of attack, while generally keeping within balance loading restrictions. In each case, force data were measured at cavitation numbers of 2.04, 1.26, 0.90, 0.53, 0.33 and 0.22. Data were also taken for the cavitation numbers associated with incipient and desinent cavitation.

When the cavity extended past mid-chord, large unsteady forces developed, with peaks observed by oscilloscope to be two to four times steady state. These overloaded the balance and made it impossible to make measurements over the wide ranges of flap angle and angle of attack originally planned. An additional restriction occurred at high flap angles, when the working section pressures required to suppress cavitation exceeded the maximum allowable.

## 5. CORRECTIONS AND ACCURACY

The force balance, manometer, physical constants and other data were recorded on punched cards and reduced using digital computer processing.

The balance zero values were dependent on the model attitude, making corrections necessary for these "gravity tare" values for each run. The measured data were also corrected for the effect of balance interactions by the application of an inverse calibration matrix. Finally, the data were corrected for the influence of the forces acting on the fairing disc, the "balance tares". These were determined for each model test condition using the following procedure. The model was removed from the force balance, inverted and installed in a support fixture on the opposite wall. A dummy fairing disc was then mounted on the force balance and the tip of the model brought to within 0.002 inch of the disc. This clearance was maintained by mechanically adjusting the hydrofoil model to compensate for changes due to working section pressure. The disc forces could then be measured for each test condition in flow conditions similar in many respects to those applying in practice.

These balance tare values were reasonable for lift and moment, representing at their worst, less than 1% and 3% of the maximum recorded values. This was not the case for the drag measurement. Maximum drag tare values were about 25% of maximum recorded drag and appear to have varied systematically with tunnel pressure. This is illustrated in Figure 7 which shows the drag tare values for the $0°\alpha$, $0°\delta$ and $0°\alpha$, $5°\delta$ cases plotted against tunnel pressure for various speeds. The tare measurement arrangement was a close approximation to and not an exact duplication of measurement conditions, and it is difficult to say what influences were present in practice. The fact that drag tare values could be large and variable is considered to prejudice significantly the reliability of the drag results.

No tunnel boundary corrections were applied and there were no corrections for model deflections under load.

Manometer indications of velocity in the working section exhibited a fluctuation which varied from approximately $\pm$ 0.5% at 10 ft/sec to $\pm$ 1% at 60 ft/sec. The period was long and there were frequent occasions when the reading was virtually steady. Data were recorded during these occasions and as a result, velocity data presented here are believed accurate to within $\pm$ 0.5%. Working section pressure indicators exhibited similar, though smaller, fluctuations and these measurements are also believed accurate to within $\pm$ 0.5%.

CIT estimates for other total measurement errors are as follows:

angle of attack: $\pm$ 0.1 deg

data reduction: $\pm$ 0.1% of indicated value

lift force: $\pm$ 2.1 lbs, giving

$C_\ell = \pm .0035$ at 50 ft/sec

pitching moment: $\pm$ 3.1 in-lbs, giving

$C_m = \pm .0051$ at 50 ft/sec

## 6. DISCUSSION OF RESULTS

### 6.1 General Note on Boundary Layer Flow Conditions and Effects

The NACA 16 Series section is designed to have an extensive region of laminar flow for a range of lift coefficients

around the design value, giving comparatively low drag under normal steady state conditions. The location of the point of transition to turbulent flow moves forward suddenly when $C_\ell$ is either decreased or increased beyond the laminar range, leading to a sharp increase in drag. Flow is then said to have become turbulent. The range of $C_\ell$ values for which laminar flow conditions are realised becomes narrower with increasing Reynolds number.

The companion series of wind tunnel tests[4] shed considerable light on the boundary layer conditions applying to the wind and water tunnel models. Laminar flow conditions were obtained as expected in the wind tunnel but there was an additional complication because transition to turbulent flow was accompanied by flow separation over the trailing edge of the flap. This in turn led to sharp decreases in the effective camber of the section, decreasing the section lift. The largest decreases occurred for higher flap angles at the positive limit of the laminar $C_\ell$ range but similar, smaller changes occurred at the negative limit.

Wind tunnel lift coefficients are shown plotted against angle of attack in Figure 8, both with and without roughness strips. Application of roughness strips to the upper and lower surfaces of the section at the 5% chord points fixed the points of transition over the whole $C_\ell$ range and established the turbulent flow condition artificially. This changed the nature of the force and moment characteristics because trailing edge separation then took place comparatively smoothly with increasing and decreasing flap angle and angle of attack. The lift values were reduced over the formerly unseparated range but the sharp discontinuities associated with delayed transition to turbulent flow were eliminated.

The lift data from the water tunnel are also shown in Figure 8. These have values which lie between the transition-fixed and transition-free wind tunnel data, over the formerly unseparated part of the wind tunnel range of angles of attack. The indications are that for the water tunnel model, separation spread smoothly over the trailing edge with increasing angle of attack in a manner somewhat similar to the transition-fixed wind tunnel model. The reason for this is not clear since the free stream turbulence levels are thought to be similar in both facilities and chord Reynolds number was lower in the water tunnel. However the surface roughness Reynolds number may well have been higher for the water tunnel model. This and the relatively large section profile errors could have been factors in promoting more rapid transition and spread of trailing edge separation.

## 6.2 Lift Characteristics

Lift coefficient is plotted against angle of attack in Figure 9 for the full range of flap angles and for a cavitation number of 2.04, representing the largely uncavitated condition. The curves are linear for small ranges of angle of attack and flap angle, but show a trend to increasing non-linearity as angle of attack and flap angle approach the test range limits. The zero-lift angle of -2.1° for 0° flap angle is less negative than that obtained in both the available sets of wind tunnel data[1,4] which gave a value of -2.6° for the transition-free test condition. The non-linearity of the data and less negative zero-lift angle are both attributed to flow separation over the trailing edge of the flap, as discussed earlier in Section 6.1.

Lift coefficient is shown plotted against flap angle with angle of attack as a parameter in Figure 10, for the same cavitation number of 2.04. The curves depart substantially from linear for both positive and negative flap angle, again apparently as a result of flow separation on the upper or lower surface of the flap.

The typical effect of cavitation number on lift coefficient at 0° angle of attack is shown in Figure 11 for the full range of flap angles. The cavitation inception limit lines on the diagram show that leading edge cavitation could be followed by an increase in lift as cavitation number decreased (see also Figures A13 to A19 in Appendix A). Presumably the effect of a small amount of leading edge cavitation was to increase the effective section camber. As the cavitation number of the flow was decreased, cavitation spread chordwise over the section until it reached the mid-back or hinge-line when the forces tended to become very unsteady. Marked decrease of lift coefficient was normally associated with extension of hinge-line or leading edge cavitation beyond the trailing edge, when the effective camber would be much decreased.

The travelling, growing bubble type of cavitation was the type most often observed but at high angles of attack or flap angle, sheet cavitation could occur in a band at the leading edges of both the foil and flap.

The foil and flap lift-curve slopes are plotted against flap angle in Figure 12. These are defined as the rates of change of lift coefficient with angle of attack and flap angle respectively and are shown for the uncavitated condition at 0° angle of attack. The foil lift-curve slope has

a value of 0.096 per degree for a small range of flap angles close to 0° (about 4% less than the corresponding wind tunnel value) but falls off sharply for flap angles greater than 5°. The flap lift-curve slope has a maximum value of about 0.06 for a very small range of flap angles close to zero.

The corresponding flap effectiveness ratios, defined as the ratio of flap lift-curve slope to foil lift-curve slope, are plotted in Figure 13 for a constant lift-curve slope of 0.096 per degree. The theoretical value can be approximated for the unseparated flow condition by[7]

$$\frac{C_{\ell\delta}}{C_{\ell\alpha}} = \frac{4}{\pi}\sqrt{f} = 0.64$$

This value is achieved, but only for a very small range of flap angles close to zero.

### 6.3 Drag Characteristics

Drag coefficient is plotted against lift coefficient in Figure 14 for a range of flap angles at a cavitation number of 2.04. Data from the companion wind tunnel tests, included for comparison, show the water tunnel data to be higher in value except for a small range of $C_\ell$ values close to the design point. The wind tunnel values were obtained for a large, accurate model, using the comparatively precise wake survey method. Despite the care taken with the water tunnel force and moment measurements, the balance and the model mounting arrangements seem likely to have introduced errors, as indicated by the comparatively large drag tare values mentioned in Section 5. Consequently, with the exception of Figures 14 and 19 no drag data are included here.

### 6.4 Moment Characteristics

The quarter-chord pitching moment, $C_m$, is plotted as a function of lift coefficient in Figure 15 for the range of flap angles at a cavitation number of 2.04. $C_m$ can be expected to become more negative as flap angle increases owing to the increase in effective camber. The rate of change can be estimated from the thin aerofoil theory of Glauert[8] as

$$C_{m\delta} = -2\sqrt{f(1-f)^3} = -0.011 \text{ per degree.}$$

Figure 15 shows that a $C_m$ change of approximately 0.055 results from a 5° flap angle change at values of $C_\ell$ close to 0.2. How-

ever, there is also a marked change of $C_m$ with $C_\ell$. This is presumably due to increasing separation and straightening of the flow. Because of this, a 22% chord location for the aerodynamic center appears to be a better compromise than the standard value of 25% for an unflapped section.

Figure 16 shows the effect of flow cavitation number on pitching moment coefficient for 0° angle of attack. The data are generally consistent with the lift data, increasing sharply as cavitation number decreases to very low numbers, but not necessarily changing immediately with the onset of cavitation.

### 6.5 Reynolds Number Dependence of Force and Moment Coefficients

The variation of lift with Reynolds number is shown in Figure 17 for the four foil and flap angle combinations given by $\alpha = 0°$ and 2° and $\delta = 0°$ and 5°. The lift values for the $0°\alpha$, $5°\delta$ case show a comparatively sharp decrease with increasing Reynolds number. This is seen from Figure 8 to be a likely result of increased flow separation at the flap trailing edge.

There is little change at the other angle settings. Figure 8 shows that any change due to increasing separation at the 0° flap angle settings would be comparatively small. At $2°\alpha$, $5°\delta$, flow separation is apparently well established even at the lowest Reynolds number setting.

The corresponding quarter chord pitching moment data of Figure 18 are generally consistent with this analysis. There is a small increase in the 0° flap angle data values with Reynolds number, while the $0°\alpha$, $5°\delta$ values approach those for the $2°\alpha$, $5°\delta$ setting. This is to be expected since quarter chord pitching moment coefficients are dependent on effective section camber and will be similar for the same flap angle, when the boundary layer conditions are similar.

The variation of drag coefficient with Reynolds number is shown in Figure 19 for the $0°\alpha$, $0°\delta$ case, the only angle setting combination for which the drag data may be reasonably representative. The $C_d$ values increase with Re for $Re < 2.49 \times 10^6$ and then tend to follow the well-established trend line[7] for smooth surfaces in turbulent flow, indicating that at this angle setting, transition to turbulent flow occurs at about $Re = 2.49 \times 10^6$.

## 6.6 Reynolds Number Dependence of Cavitation

Tests were made for cavitation dependence on Reynolds number at the same four angle settings, using the procedure described in Section 4. The flow cavitation numbers at which inception and desinence occurred are plotted in Figure 20 for the $0°\alpha$, $0°\delta$ setting. For this case, cavitation took place virtually simultaneously on the upper surface at the flap hinge-line and at section mid-back, with little hysteresis and virtually no variation with Reynolds number.

For the $\alpha = 0°$, $\delta = 5°$ case, shown in Figure 21, hinge-line cavitation occurred first as cavitation number was decreased, followed for $Re \leq 2.49 \times 10^6$ by mid-back cavitation. For $Re > 2.49 \times 10^6$, however, although hinge-line cavitation still occurred first, it was followed by leading edge cavitation. For this particular setting, wind tunnel data show the pressure distribution to be very flat over the first half of the chord, so that little change would be required in the flow to alter the cavitation characteristics. In fact, the lift and moment coefficient values undergo fairly large changes with Reynolds number, as noted in Section 6.5 above, indicating a significant change to the flow pattern. In these circumstances, the switch from mid-back to leading edge cavitation is not surprising.

Cavitation took place only at the upper surface leading edge for the $\alpha = 2°$, $\delta = 0°$ setting, as shown in Figure 22. Some of the data exhibit considerable hysteresis and there are large differences between the data points obtained during the Reynolds number survey and those obtained during the general survey at $Re = 2.49 \times 10^6$. There are too few data points to establish the trends with certainty but the cavitation inception number appears to switch in value over the Reynolds number test range, with some uncertainty at intermediate Re values.

Cavitation also occurred only at the upper surface leading edge for the $\alpha = 2°$, $\delta = 5°$ setting and Figure 23 indicates a strong Reynolds number dependency. For this setting, cavitation spread chordwise with decreasing Reynolds number until it reached the mid-back when it spontaneously oscillated between there and the trailing edge of the flap. The resulting violent force fluctuations prevented testing over the full Reynolds number range.

These tests for Reynolds number dependence of cavitation indicate that mid-back and hinge-line cavitation are independent of Reynolds number over the test range. Leading edge cavitation occurrence does seem to be Reynolds number dependent but there are insufficient data to assess the extent to which this dependence is systematic.

### 6.7 Cavitation Limit Diagrams

The limit lines for cavitation inception are given in Figure 24 for all flap angles tested. The hinge-line (or occasionally mid-back) limits, represented by the lower lines of the bucket curves, increase with flap angle as would be expected. The Reynolds number dependency tests described in Section 6.6 indicate that these lines will be relatively independent of Reynolds number.

The leading edge cavitation limits (represented by the right hand lines) on the other hand, will be affected by Reynolds number. They seem likely to move to the left with increasing Reynolds number, narrowing the range of uncavitated $C_\ell$ available at the higher full scale Reynolds numbers.

## 7. CONCLUSIONS

Tests on a 16-309 section equipped with a 25% flap chord ratio, simple, sealed flap show the characteristics to be influenced greatly by turbulent flow separation over the flap trailing edge. This greatly decreases the lift available over much of the normal range of flap angle and angle of attack.

Values of foil lift-curve slope and flap effectiveness are close to theoretical at 0° flap angle but decline fairly rapidly as flap angle increases or decreases.

The drag coefficient data are unduly high and are considered suspect except for a narrow range of lift coefficients between about zero and 0.25. The reason for this is not known but may have been due to difficulties in accounting for balance tares.

The pitching moment data indicate the aerodynamic center to be at about 0.22 chord. For flap angles greater than 5°, considerable increase in the quarter chord pitching moment coefficient occurs with increasing $C_\ell$.

Comparison with companion wind tunnel test data, together with Reynolds number sensitivity tests indicate that transition to turbulent flow occurs fairly readily in the water tunnel. Turbulent flow is well established on the model at the main test Reynolds number of $2.49 \times 10^6$ but the indications are that some forward movement of the transition point continues as Reynolds number is increased.

Despite well-established turbulent flow, leading edge cavitation occurrence is sensitive to Reynolds number, making the data useful only as a general guide to full-scale

performance. Mid-back and hinge-line cavitation proved to be insensitive to Reynolds number over the test range.

For the higher angle of attack cases, where leading edge cavitation occurs well ahead of mid-back or hinge-line cavitation as cavitation number decreases, leading edge cavitation does not lead to immediate loss of lift or increase of drag. Marked force and moment changes are more normally associated with the extension of the mid-back or hinge-line cavity beyond the trailing edge.

## ACKNOWLEDGEMENT

The tests described in this report were made at the California Institute of Technology under DSS Contract No. 8SR5-004, sponsored by the Defence Research Establishment Atlantic, Dartmouth, Nova Scotia, Canada. The section coordinates of the model were specified by DREA but the model was designed by and constructed to the requirements of CIT, which also provided the survey of the model geometry. The data were collected, corrected for tares and other effects and tabulated by CIT.

Our thanks are due to Mr. T.M. Ward of the Graduate Aeronautical Laboratories of CIT who acted as program manager for these tests, worked up the experimental techniques and wrote the original report from which the sections in this report on model description, facilities and procedures have been largely drawn.

TABLE I: NACA 16-309 HYDROFOIL MODEL COORDINATES

| $x_c$ (ins) | $y_u$ (ins) | $y_\ell$ (ins) |
|---|---|---|
| 0.000 | 0.00301 | 0.00301 |
| 0.001 | 0.00987 | -0.00385 |
| 0.002 | 0.01260 | -0.00658 |
| 0.003 | 0.01463 | -0.00861 |
| 0.004 | 0.01628 | -0.01026 |
| 0.005 | 0.01767 | -0.01165 |
| 0.006 | 0.01890 | -0.01286 |
| 0.007 | 0.02007 | -0.01292 |
| 0.008 | 0.02122 | -0.01488 |
| 0.009 | 0.02235 | -0.01574 |
| 0.012 | 0.02561 | -0.01814 |
| 0.015 | 0.02871 | -0.02038 |
| 0.018 | 0.03165 | -0.02248 |
| 0.024 | 0.03715 | -0.02628 |
| 0.030 | 0.04219 | -0.02965 |
| 0.045 | 0.05322 | -0.03660 |
| 0.060 | 0.06253 | -0.04207 |
| 0.075 | 0.07056 | -0.04657 |
| 0.090 | 0.07761 | -0.05050 |
| 0.120 | 0.08964 | -0.05729 |
| 0.150 | 0.10008 | -0.06299 |
| 0.180 | 0.10978 | -0.06798 |
| 0.210 | 0.11887 | -0.07243 |
| 0.240 | 0.12742 | -0.07652 |
| 0.270 | 0.13547 | -0.08005 |
| 0.300 | 0.14308 | -0.08339 |
| 0.360 | 0.15714 | -0.08945 |
| 0.420 | 0.16995 | -0.09487 |
| 0.480 | 0.18181 | -0.09977 |
| 0.540 | 0.19290 | -0.10424 |
| 0.600 | 0.20331 | -0.10834 |
| 0.750 | 0.22684 | -0.11730 |
| 0.900 | 0.24744 | -0.12493 |
| 1.050 | 0.26576 | -0.13175 |
| 1.200 | 0.28213 | -0.13786 |
| 1.500 | 0.30981 | -0.14812 |
| 1.800 | 0.33155 | -0.15616 |
| 2.100 | 0.34815 | -0.16244 |
| 2.400 | 0.35989 | -0.16700 |
| 2.700 | 0.36693 | -0.16979 |
| 3.000 | 0.36927 | -0.17073 |
| 3.300 | 0.36680 | -0.16964 |
| 3.600 | 0.35900 | -0.16609 |
| 3.900 | 0.34527 | -0.15954 |
| 4.200 | 0.43496 | -0.14943 |
| 4.500 | 0.29735 | -0.13524 |
| 4.800 | 0.26130 | -0.11674 |
| 5.100 | 0.21580 | -0.09375 |
| 5.400 | 0.16086 | -0.06602 |
| 5.700 | 0.09310 | -0.03456 |
| 6.000 | 0.00540 | -0.00504 |

TABLE II: TEST CONDITION SUMMARY

| ANGLE (DEGS) | WATER SPEED (FT/SEC) | WINDOW TYPE ANGLE OF ATTACK (DEGS) -5 | -4 | -3 | -2 | -1 | 0 | 1 | 2 | 3 | 4 | 6 | SURVEY TYPE | REMARKS |
|---|---|---|---|---|---|---|---|---|---|---|---|---|---|---|
| -10 | 50 | | | | | | P | P | | | | | Cavitation | |
| - 5 | 50 | | | | P | | P | P | | | | | Cavitation | |
| 0 | 50 | | P | | P | P | P | P | P<br>A | | P | A | Cavitation | Flow State Photographs |
| 2.5 | 50 | A | A | | A | | A | A | A | | | A | Cavitation | |
| 5 | 50 | | P | P | P | P | P | P | P | P | | | Cavitation | |
| 7.5 | 50 | A | A | | A | | A | A | A | | | | Cavitation | |
| 10 | 50 | P | P | | P | P | P | P | P | P | | | Cavitation | Flow State Photographs |
| 0 | 25,40,50,70,80 | | | | | | A | | A | | | | Reynolds No. | |
| 5 | 25,40,50,70,80 | | | | | | | | | | | | Reynolds No. | |

P - "Plexiglas" sidewall
A - Aluminum sidewall


Fig. 1: Model Ready for Installation

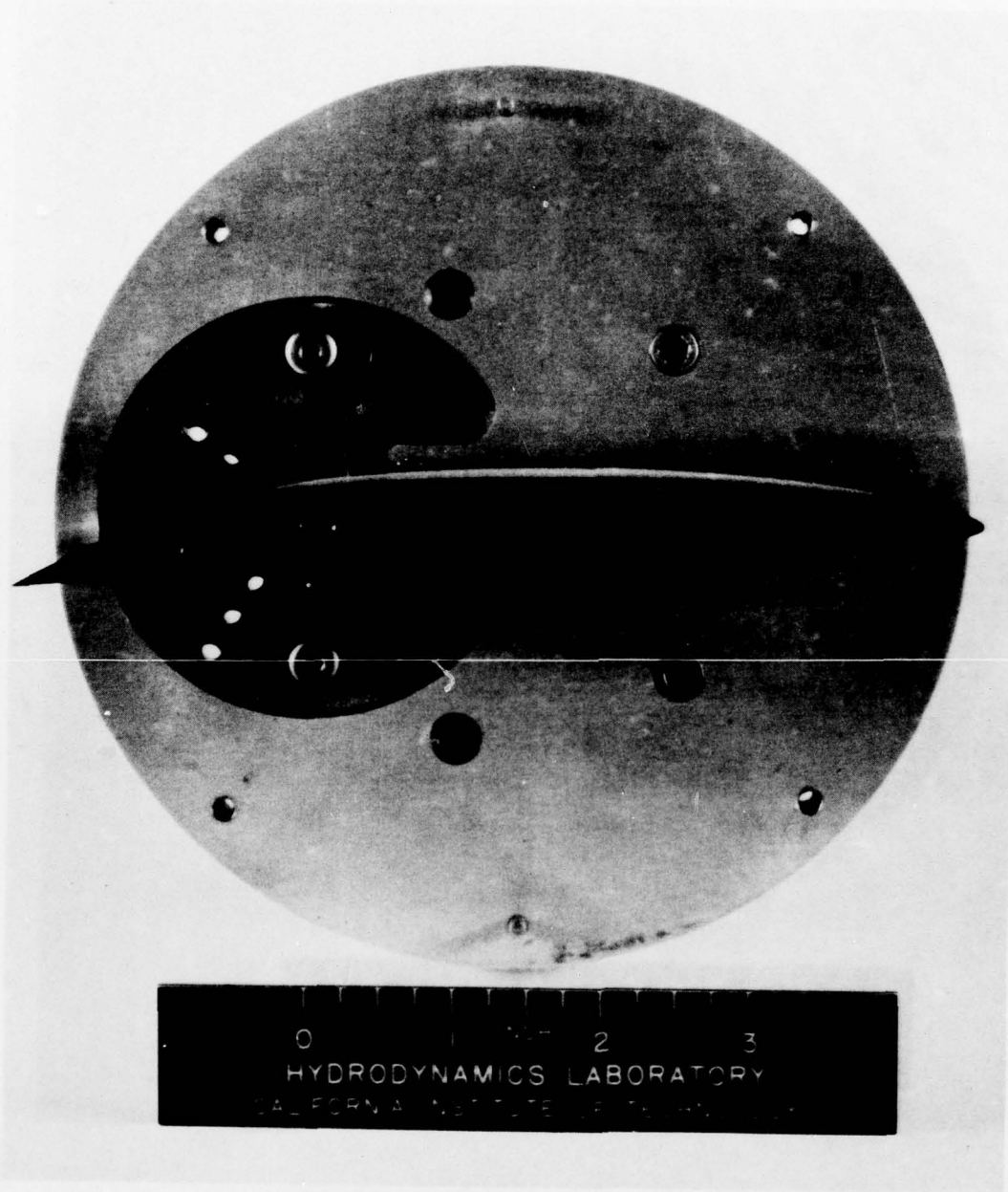


Fig. 2: Model with Fairing Plate Removed

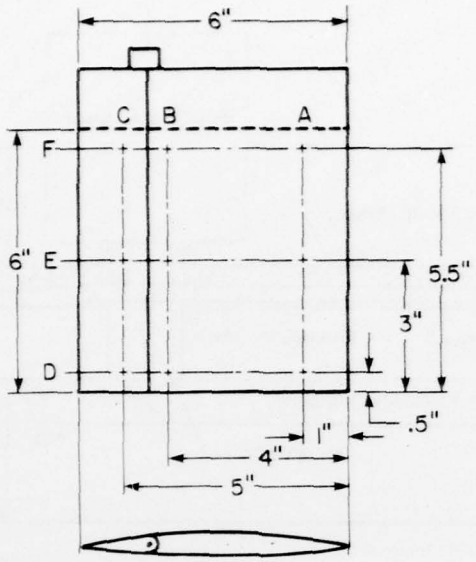


Fig. 3: Inspection Axes

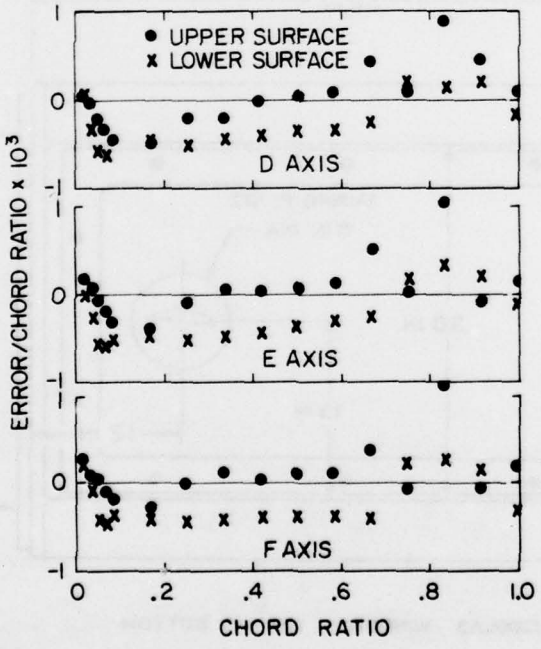


Fig. 4: Profile Deviations

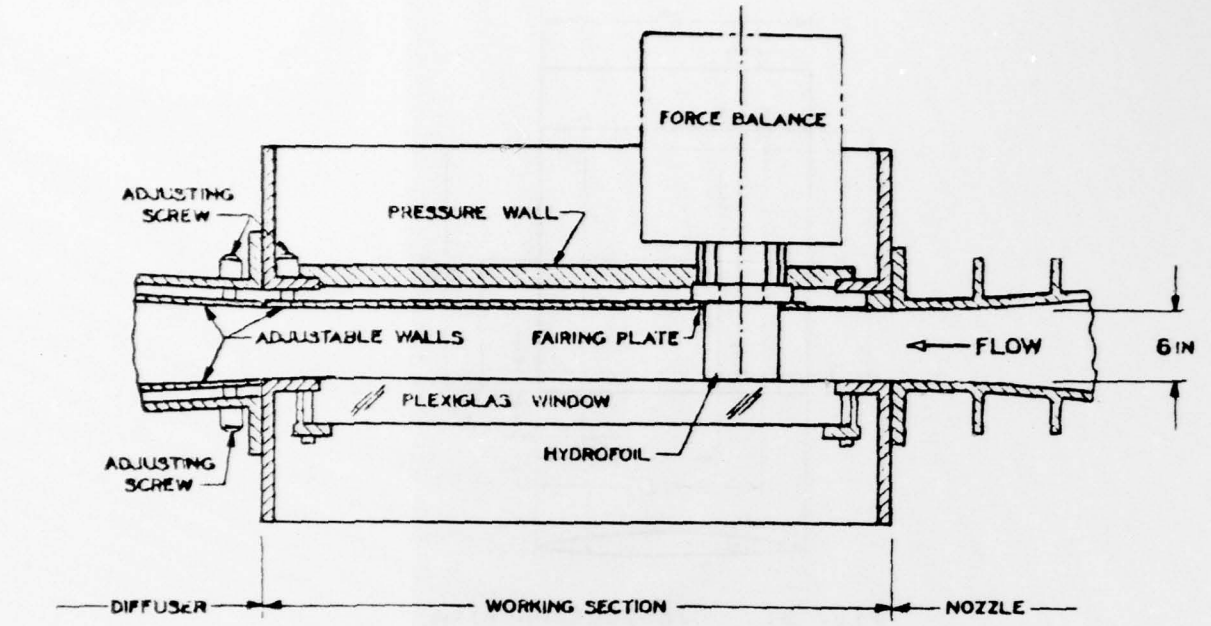


SECTION A-A

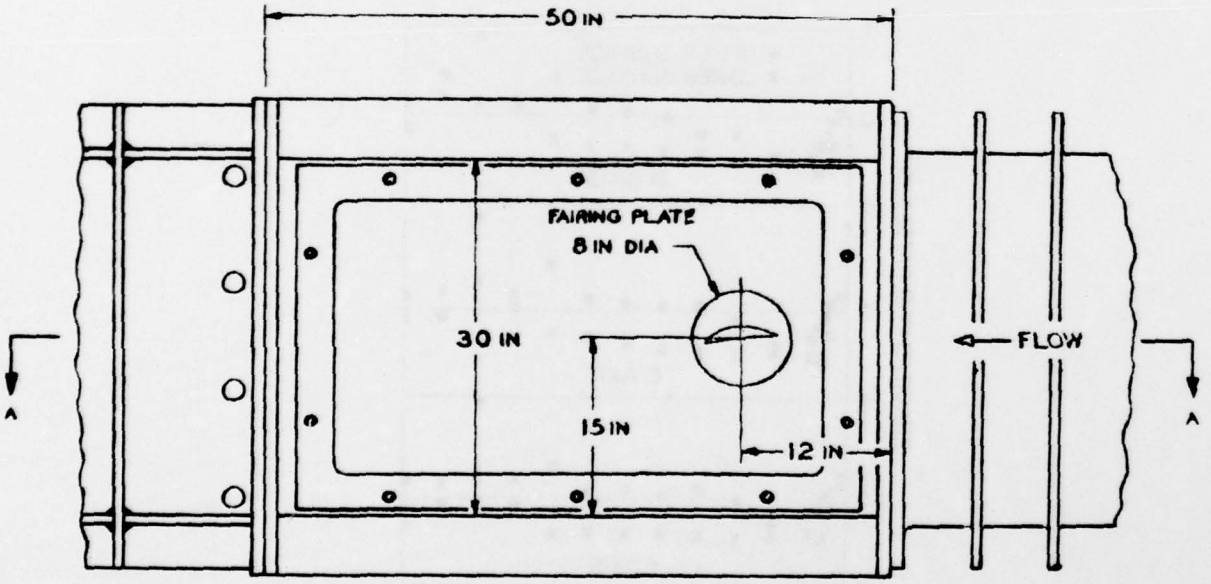


PLEXIGLAS WINDOWS TOP AND BOTTOM

Fig. 5: Two Dimensional Working Section Schematic

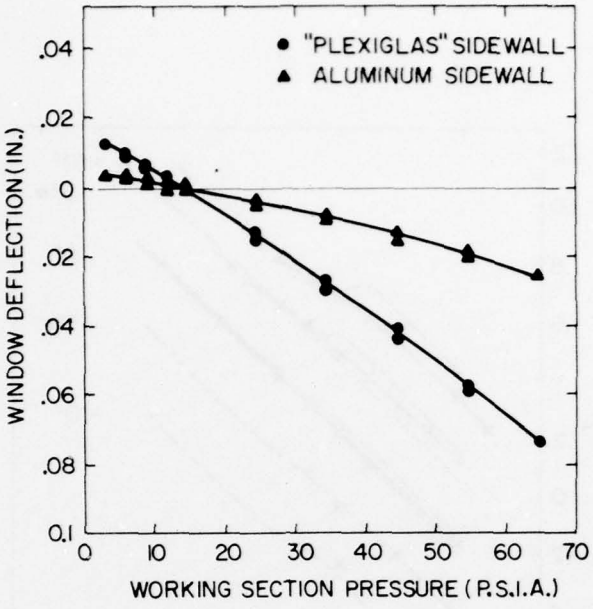


Fig. 6: Variation of Window Deflection with Working Section Pressure

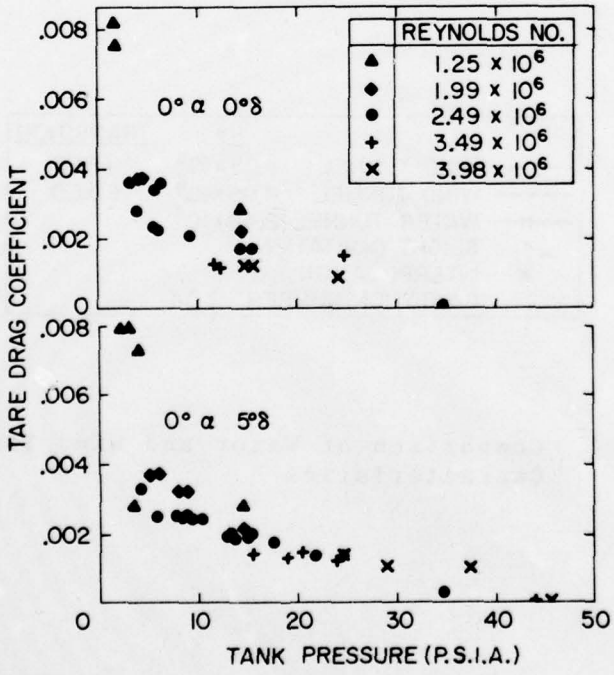


Fig. 7: Variation of Drag Tares with Tunnel Pressure

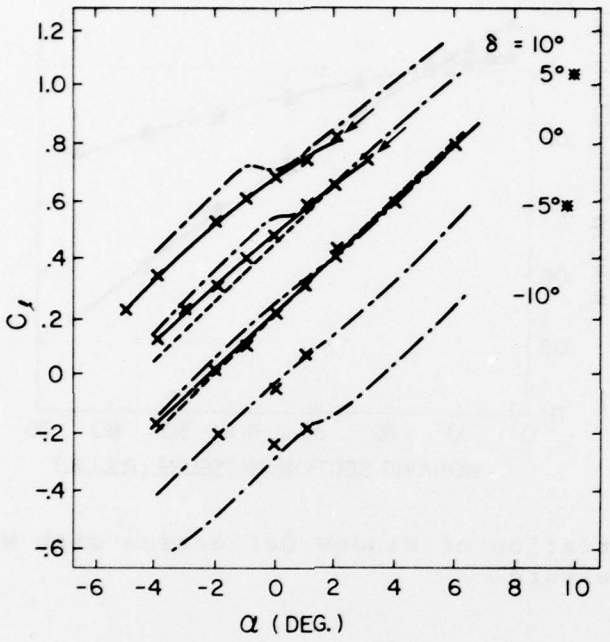


| | Re | TRANSITION |
|---|---|---|
| —·— WIND TUNNEL | $4.05 \times 10^6$ | FREE |
| - - - - WIND TUNNEL | $4.05 \times 10^6$ | FIXED |
| —×— WATER TUNNEL | $2.49 \times 10^6$ | |
| ↙ SLIGHT CAVITATION | | |
| ✱ INTERPOLATION | | |
| CAVITATION NUMBER | 2.04 | |

Fig. 8: Comparison of Water and Wind Tunnel Lift Characteristics

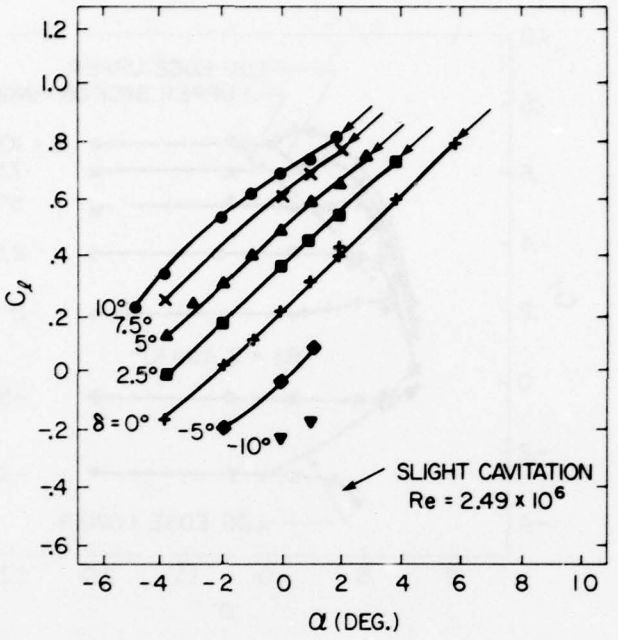


Fig. 9: Variation of Lift Coefficient with Angle of Attack for 2.04 Cavitation No.

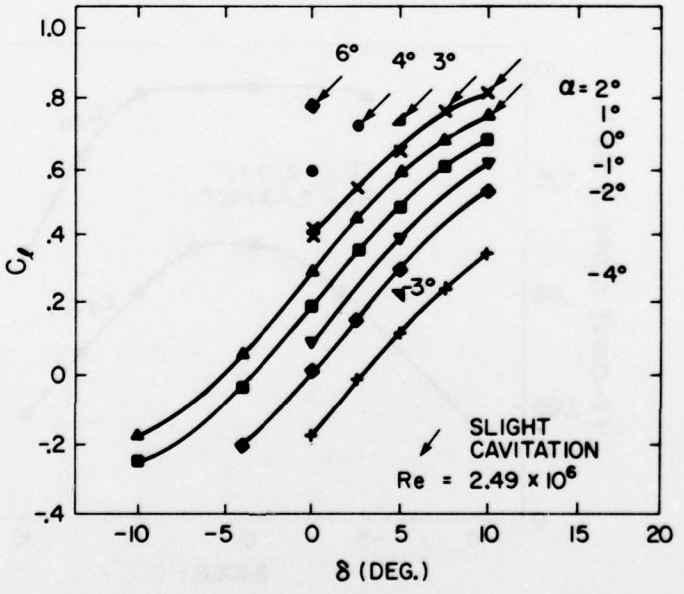


Fig. 10: Variation of Lift Coefficient with Flap Angle for 2.04 Cavitation No.

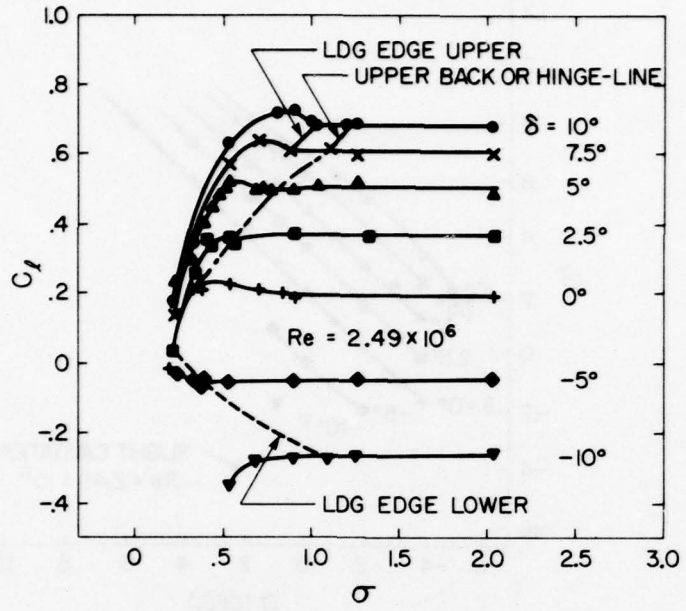


Fig. 11: Variation of Lift Coefficient with Cavitation No. at 0° Angle of Attack

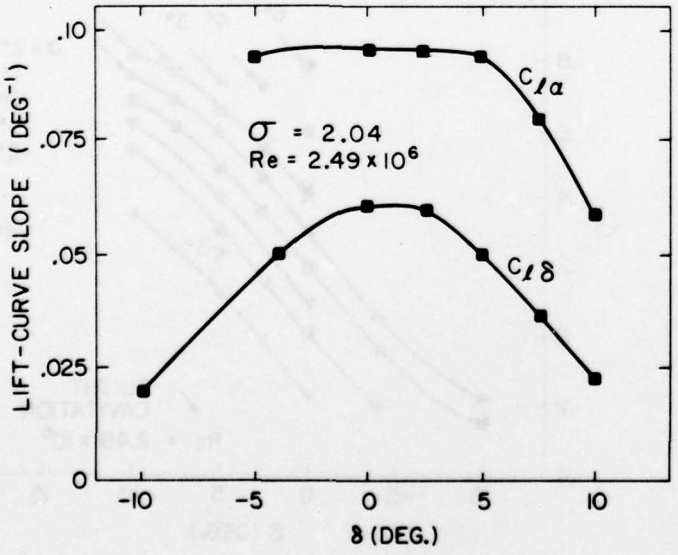


Fig. 12: Lift Curve Slopes at 0° Angle of Attack

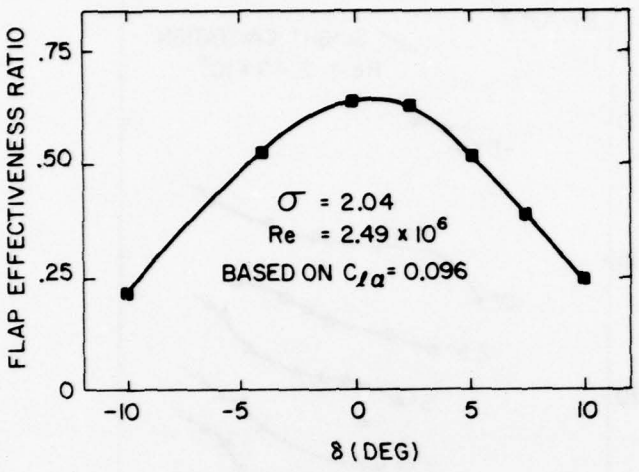


Fig. 13: Flap Effectiveness Ratio at 0° Angle of Attack

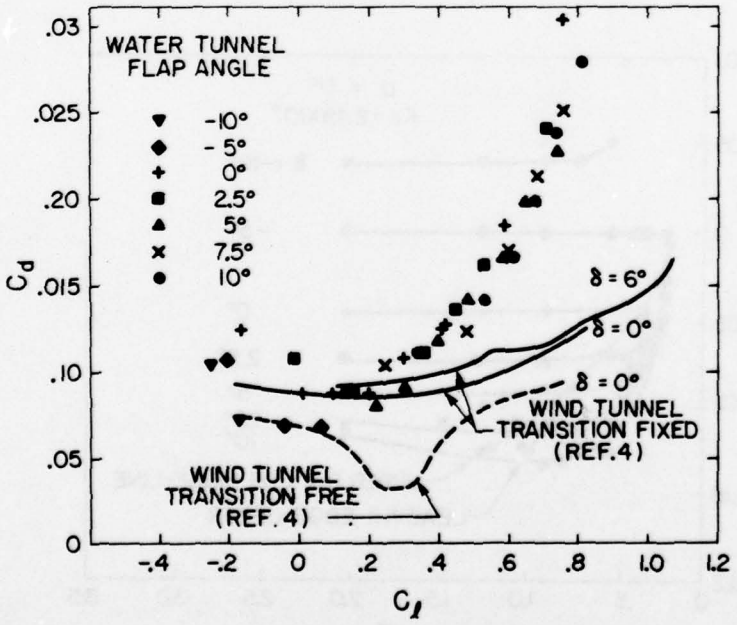


Fig. 14: Variation of Drag Coefficient with Lift Coefficient at 0° Angle of Attack

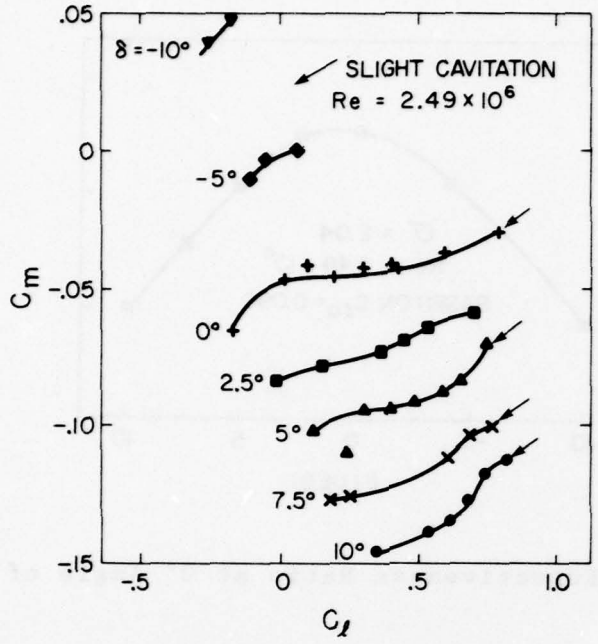


Fig. 15: Variation of Quarter Chord Pitching Moment Coefficient with Lift Coefficient at 0° Angle of Attack

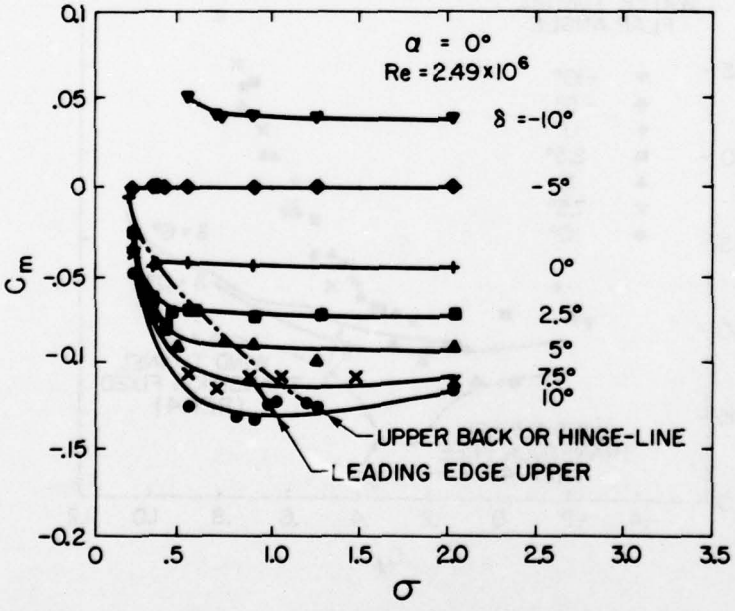


Fig. 16: Variation of Quarter Chord Pitching Moment Coefficient with Cavitation No.

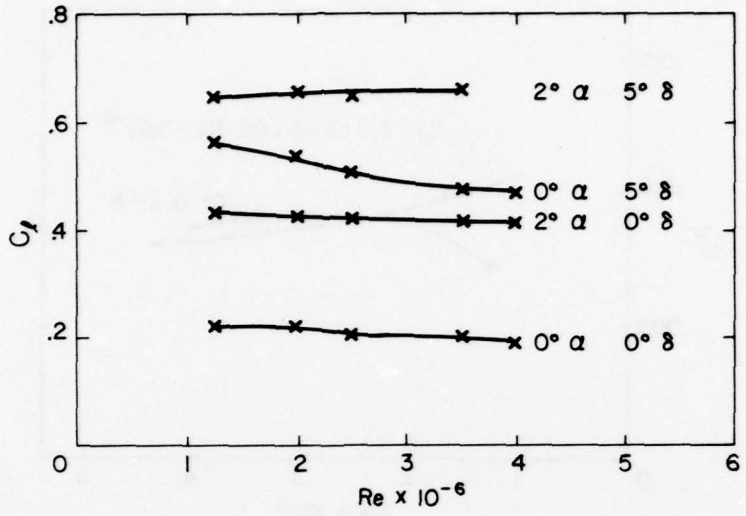


Fig. 17: Variation of Uncavitated Lift Coefficient with Reynolds No.

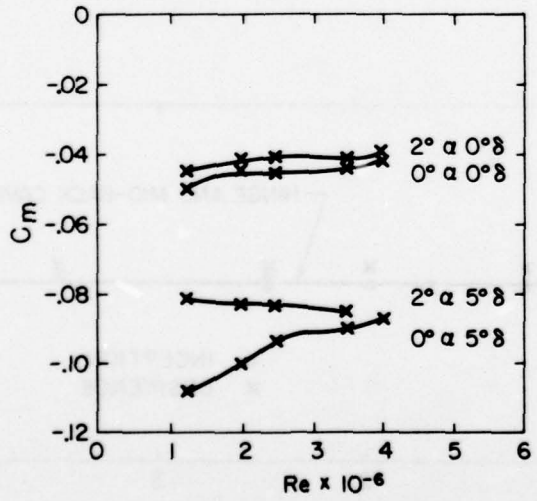


Fig. 18: Variation of Uncavitated Quarter Chord Pitching Moment Coefficient with Reynolds No.

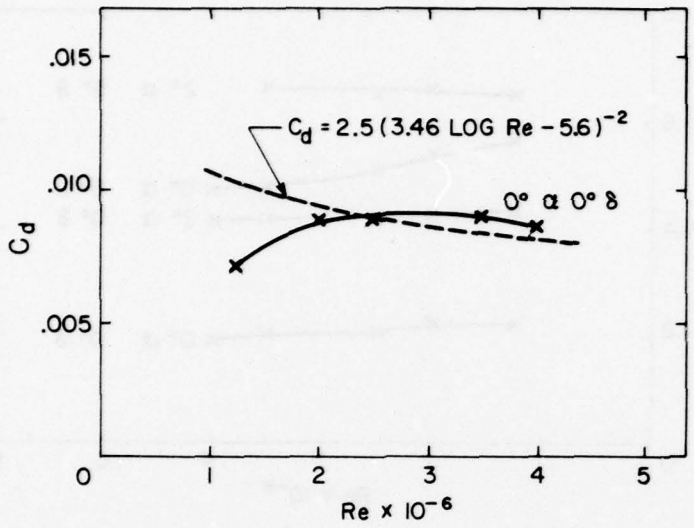


Fig. 19: Variation of Uncavitated Drag Coefficient with Reynolds No.

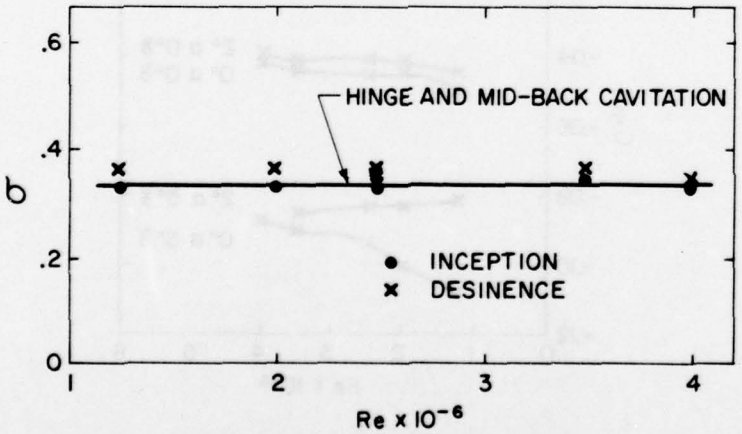


Fig. 20: Variation of Cavitation Inception with Reynolds No. for $\alpha = 0°$, $\delta = 0°$

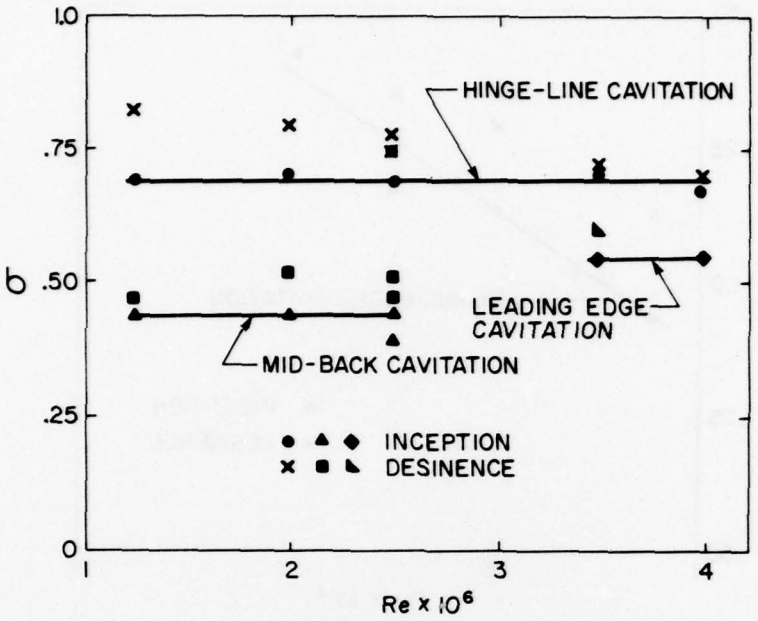


Fig. 21: Variation of Cavitation Inception with Reynolds No. for $\alpha = 0°$, $\delta = 5°$

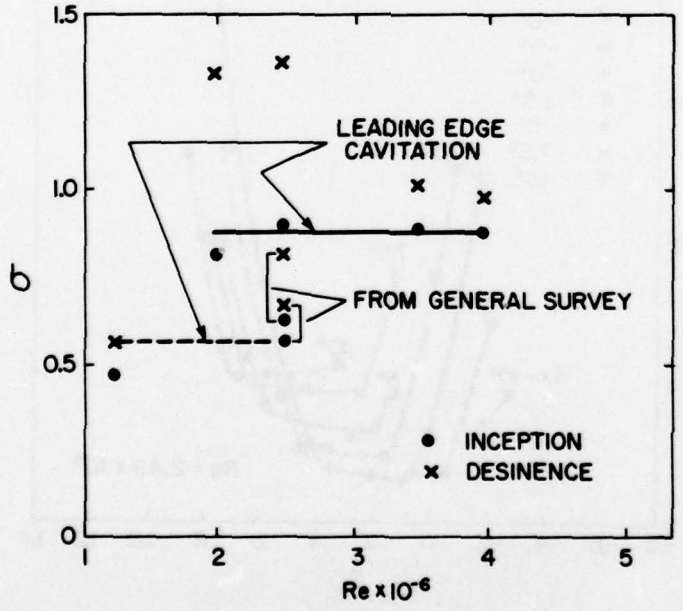


Fig. 22: Variation of Cavitation Inception with Reynolds No. for $\alpha = 2°$, $\delta = 0°$

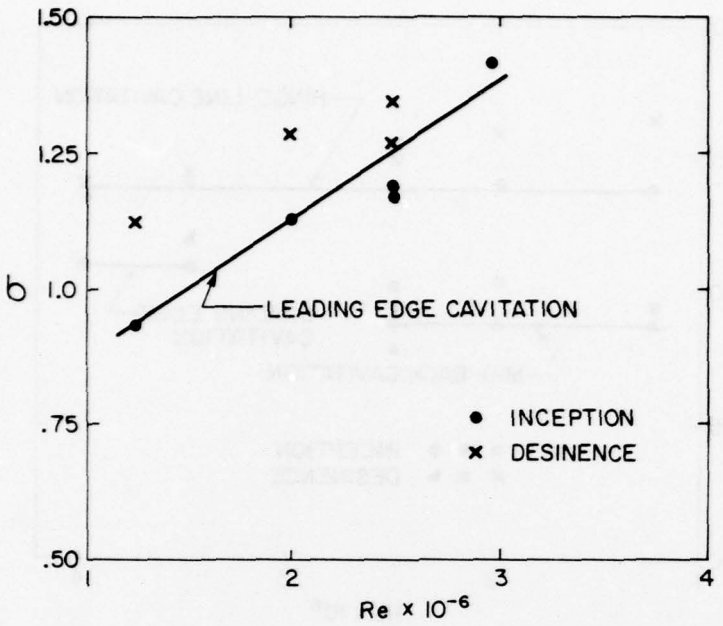


Fig. 23: Variation of Cavitation Inception with Reynolds No. for $\alpha = 2°$, $\delta = 5°$

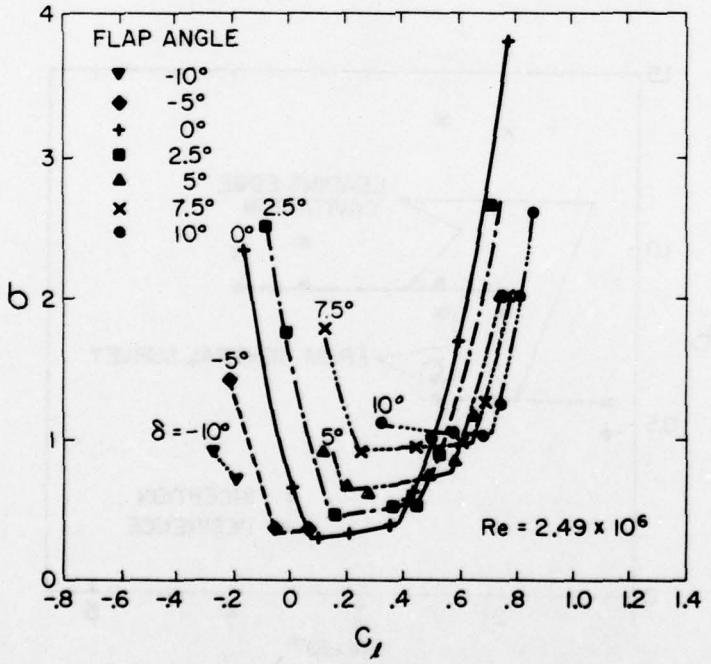


Fig. 24: Cavitation Inception Limits for Various Flap Angles.

## REFERENCES


1. Lindsey, W.F., Stevenson, D.B. and Daley, B.N., "Aerodynamic Characteristics of 24 NACA 16-Series Airfoils at Mach Numbers Between 0.3 and 0.8", Technical Note No. 1546, Langley Aeronautical Laboratory, Langley Field, Virginia, September 1948.

2. Arakeri, V.H. and Acosta, A.J., "Viscous Effects in the Inception of Cavitation on Axisymmetric Bodies", Journal of Fluids Engineering, Trans. ASME, Vol. 95, Series I, No. 4, Dec. 1973.

3. Huang, T.T. and Peterson, F.B., "Influence of Viscous Effects on Model/Full-Scale Cavitation Scaling", Journal of Ship Research, Vol. 20, No. 4, Dec. 1976.

4. "Low Speed Wind Tunnel Tests of a NACA 16-309 Section with Trailing Edge Flap", DeHavilland Aircraft of Canada Ltd., Report 76-3, October 1976, for Defence Research Establishment Atlantic, P.O. Box 1012, Dartmouth, Nova Scotia.

5. Abbott, I.H. and VonDoenhoff, W.E., "Theory of Wing Sections", Dover Publications, Inc., New York (1959).

6. Ward, T.M., "The Hydrodynamics Laboratory at the California Institute of Technology - 1976", Journal of Fluids Engineering, ASME, December 1976.

7. Hoerner, S.F., "Fluid Dynamic Lift", Hoerner Fluid Dynamics, P.O. Box 342, Brick Town, N.J., 08723.

8. Glauert, H.: "The Elements of Aerofoil and Airscrew Theory", Cambridge University Press, Second Edition, 1947.

9. Hoerner, S.F., "Fluid Dynamic Drag", Hoerner Fluid Dynamics, P.O. Box 342, Brick Town, N.J., 08723.

# APPENDIX A

## TEST DATA PLOTS

| FIGURE | TITLE |
|---|---|
| A1 | Lift Coefft-vs-Angle of Attack for 2.04 Cavitation No. |
| A2 | " " " " 1.26 " " |
| A3 | " " " " 0.90 " " |
| A4 | " " " " 0.53 " " |
| A5 | " " " " 0.33 " " |
| A6 | " " " " 0.22 " " |
| A7 | Lift Coefft-vs-Flap Angle for 2.04 Cavitation No. |
| A8 | " " " " 1.26 " " |
| A9 | " " " " 0.90 " " |
| A10 | " " " " 0.53 " " |
| A11 | " " " " 0.33 " " |
| A12 | " " " " 0.22 " " |
| A13 | Lift Coefft-vs-Cavitation No. at 4 degrees Angle of Attack |
| A14 | " " " " 2 " " " |
| A15 | " " " " 1 " " " |
| A16 | " " " " 0 " " " |
| A17 | " " " " -1 " " " |
| A18 | " " " " -2 " " " |
| A19 | " " " " -4 " " " |
| A20 | Moment Coefft-vs-Angle of Attack for 2.04 Cavitation No. |
| A21 | " " " " 1.26 " " |
| A22 | " " " " 0.90 " " |
| A23 | " " " " 0.53 " " |
| A24 | " " " " 0.33 " " |
| A25 | " " " " 0.22 " " |
| A26 | Moment Coefft-vs-Flap Angle for 2.04 Cavitation No. |
| A27 | " " " " 1.26 " " |
| A28 | " " " " 0.90 " " |
| A29 | " " " " 0.53 " " |
| A30 | " " " " 0.33 " " |
| A31 | " " " " 0.22 " " |
| A32 | Moment Coefft-vs-Cavitation No. at 4 degs. Angle of Attack |
| A33 | " " " " 2 " " " |
| A34 | " " " " 1 " " " |
| A35 | " " " " 0 " " " |
| A36 | " " " " -1 " " " |
| A37 | " " " " -2 " " " |
| A38 | " " " " -4 " " " |
| A39 | Cavitation Limit Diagram for 10 degrees Flap Angle |
| A40 | " " " 7.5 " " " |
| A41 | " " " 5 " " " |
| A42 | " " " 2.5 " " " |
| A43 | " " " 0 " " " |
| A44 | " " " -5 " " " |
| A45 | " " " -10 " " " |

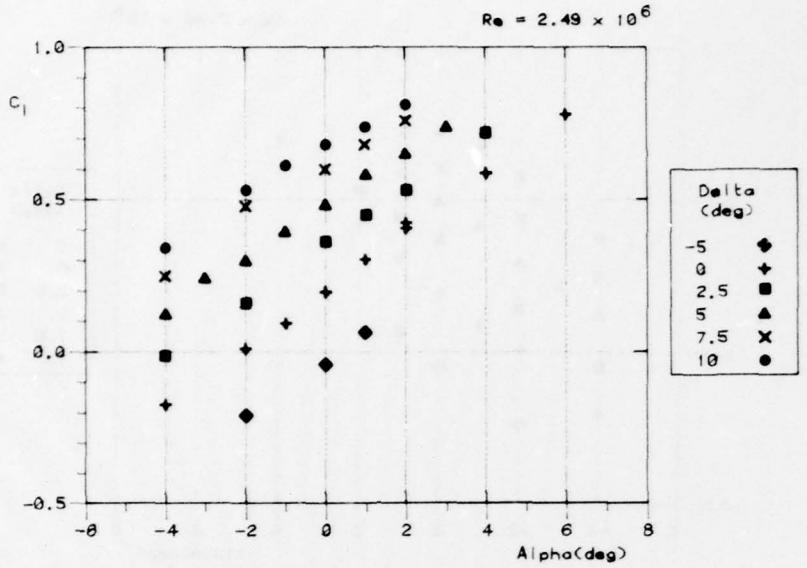


CL-VS-ALPHA FOR 2.04 CAVITATION NUMBER

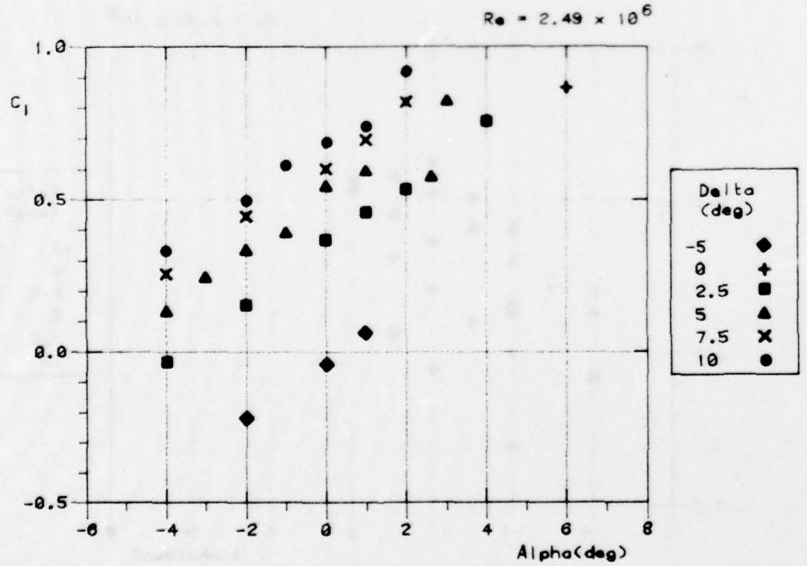


CL-VS-ALPHA FOR 1.26 CAVITATION NUMBER

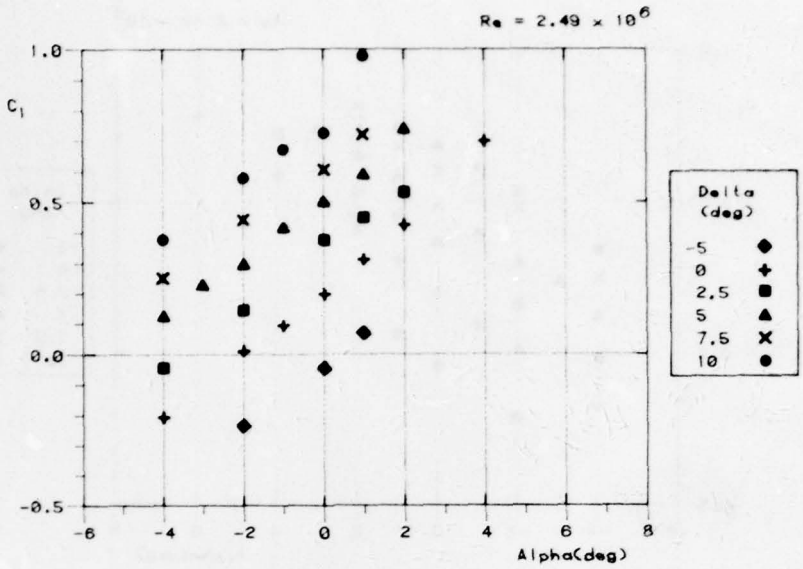


CL-VS-ALPHA FOR 0.90 CAVITATION NUMBER

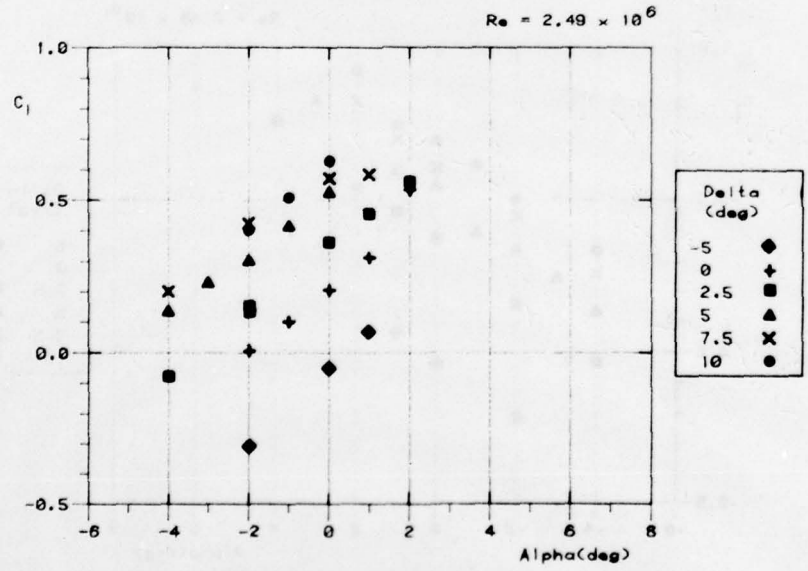


CL-VS-ALPHA FOR 0.53 CAVITATION NUMBER

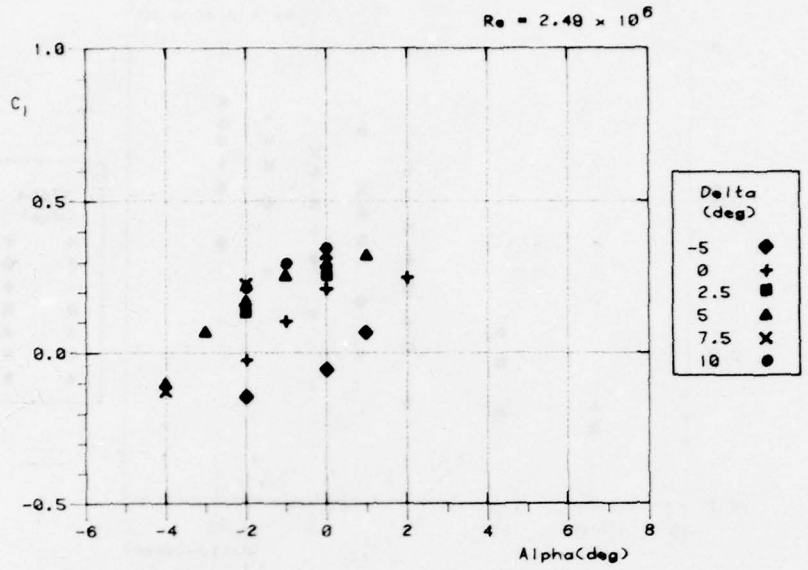


CL-VS-ALPHA FOR 0.33 CAVITATION NUMBER

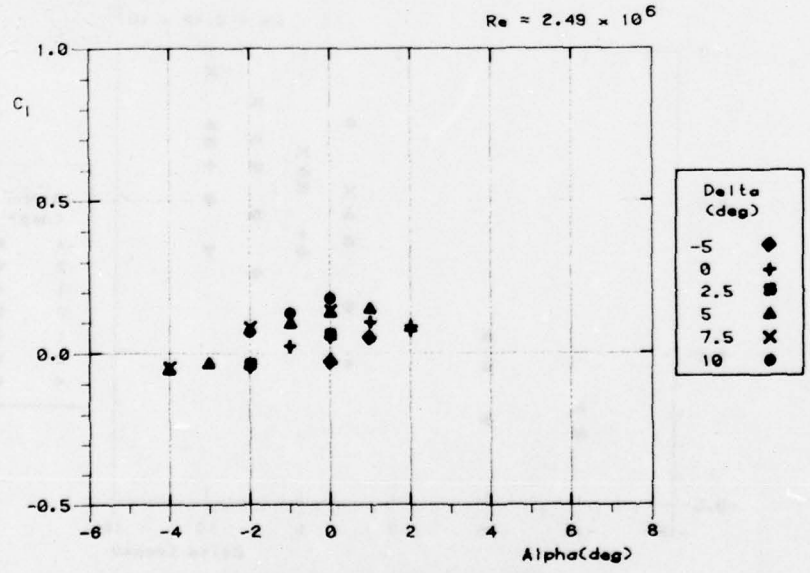


CL-VS-ALPHA FOR 0.22 CAVITATION NUMBER

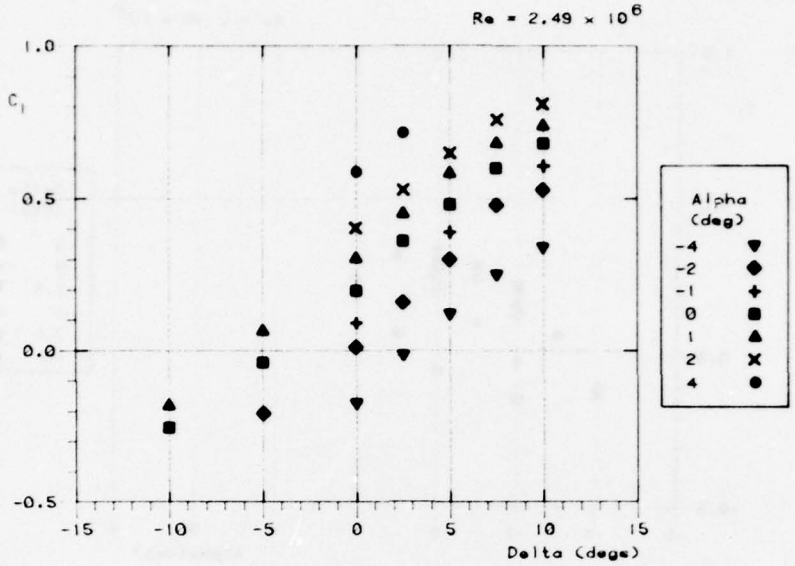


CL-VS-DELTA FOR 2.04 CAVITATION NUMBER

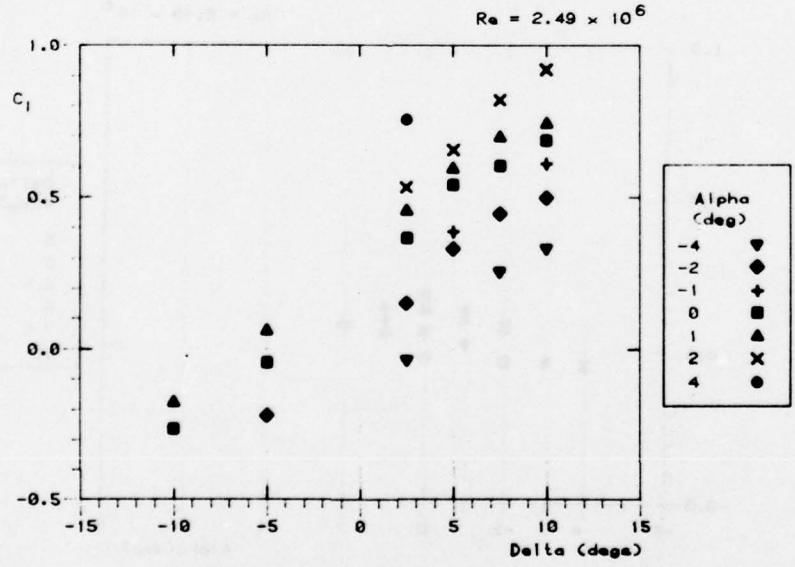


CL-VS-DELTA FOR 1.26 CAVITATION NUMBER

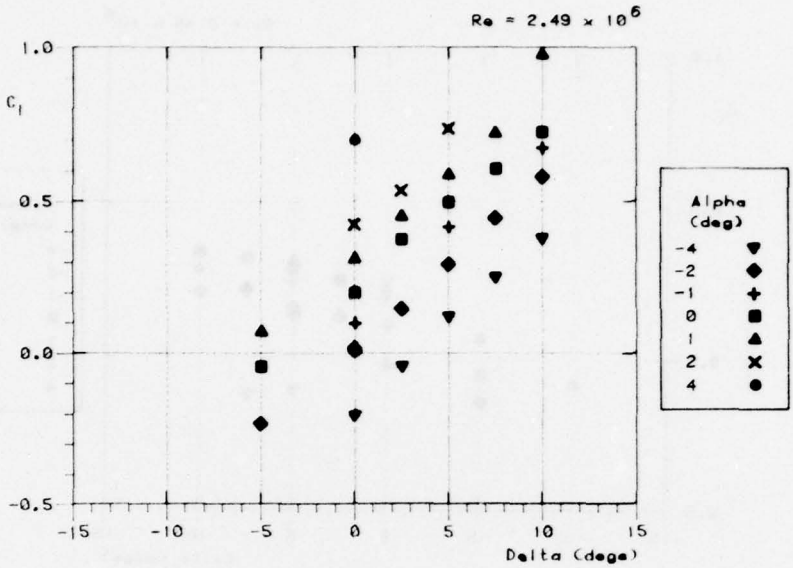


CL-VS-DELTA FOR 0.90 CAVITATION NUMBER

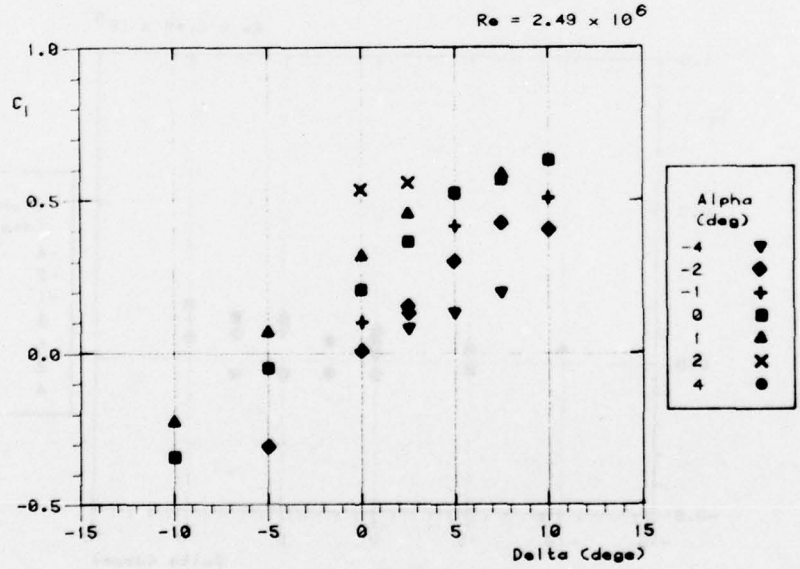


CL-VS-DELTA FOR 0.53 CAVITATION NUMBER

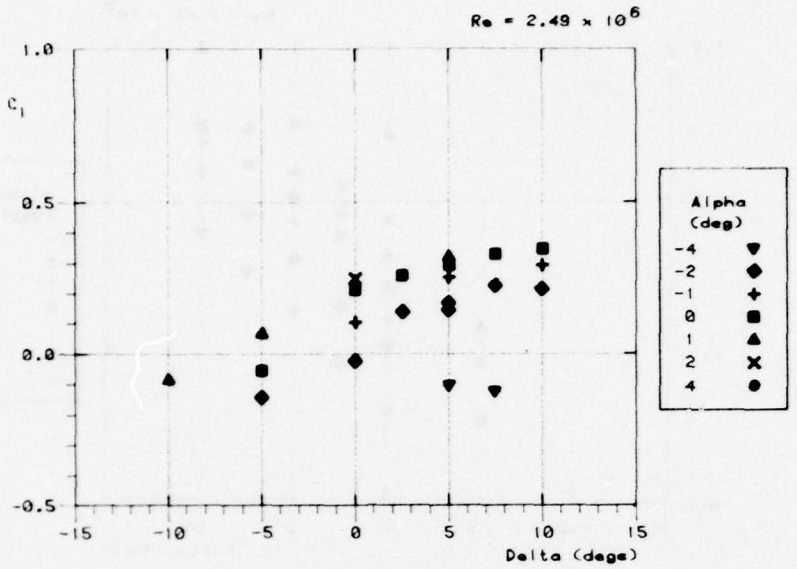


CL-VS-DELTA FOR 0.33 CAVITATION NUMBER

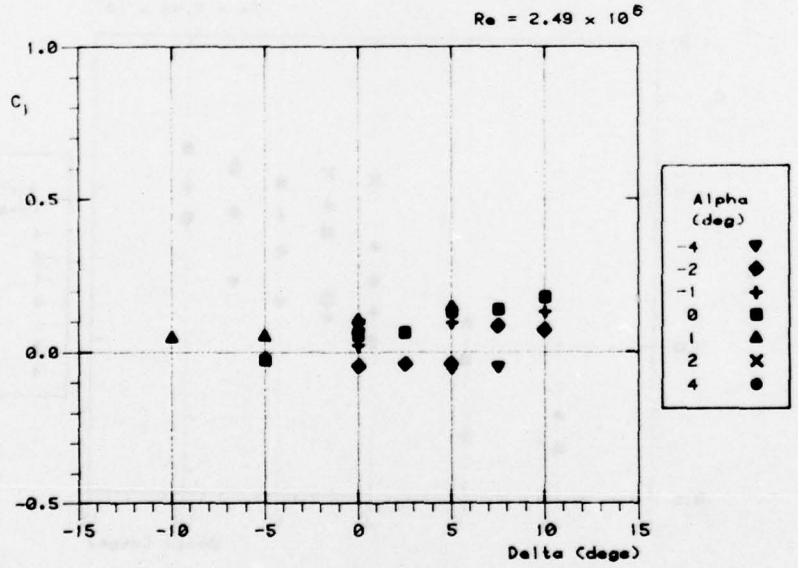


CL-VS-DELTA FOR 0.22 CAVITATION NUMBER

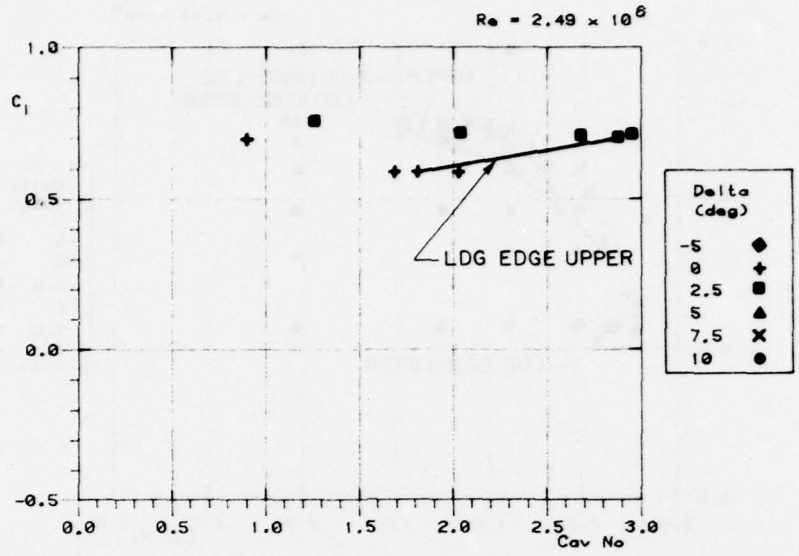


CL-VS-CAV NO AT 4 DEG ALPHA

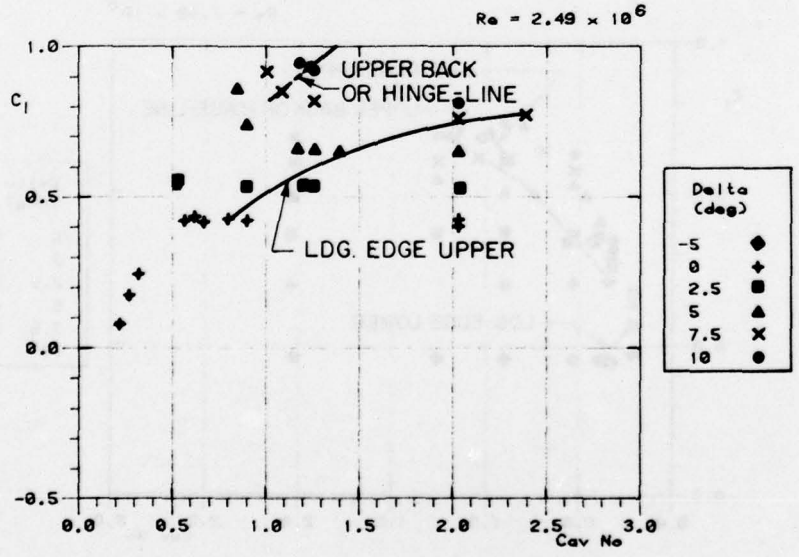


CL-VS-CAV NO AT 2 DEG ALPHA

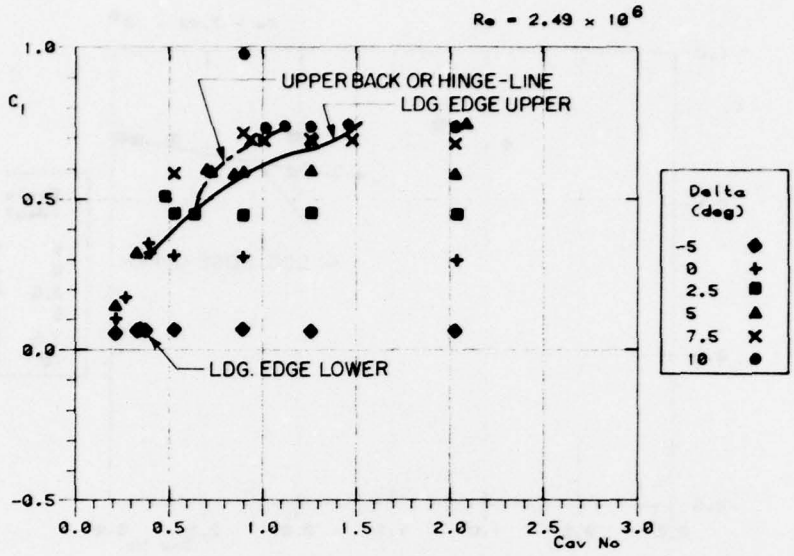


CL-VS-CAV NO AT 1 DEG ALPHA

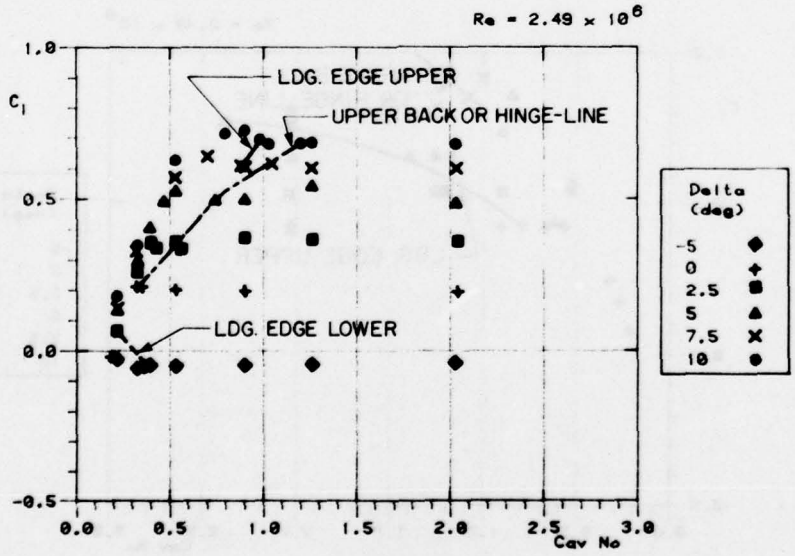


CL-VS-CAV NO AT 0 DEG ALPHA

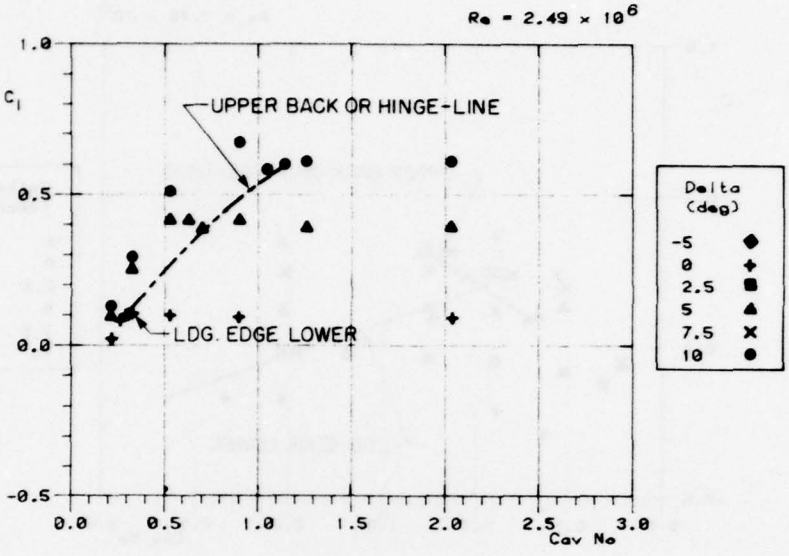


CL-VS-CAV NO AT -1 DEG ALPHA

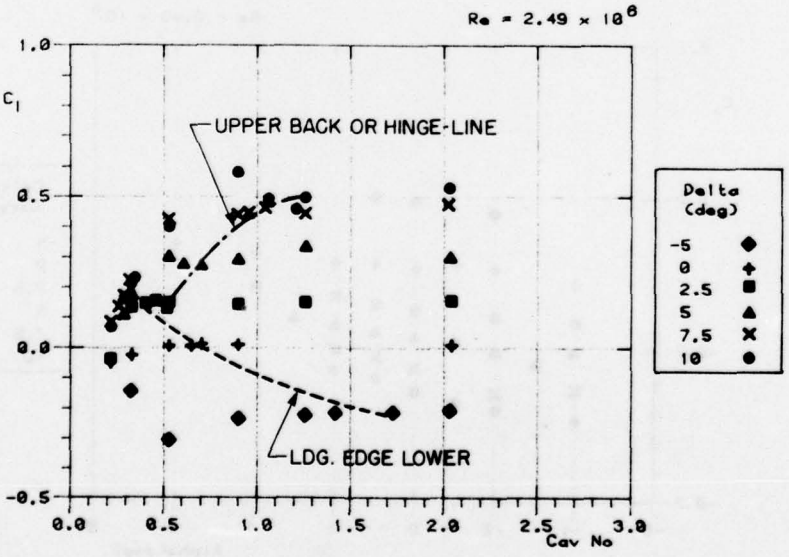


CL-VS-CAV NO AT -2 DEG ALPHA

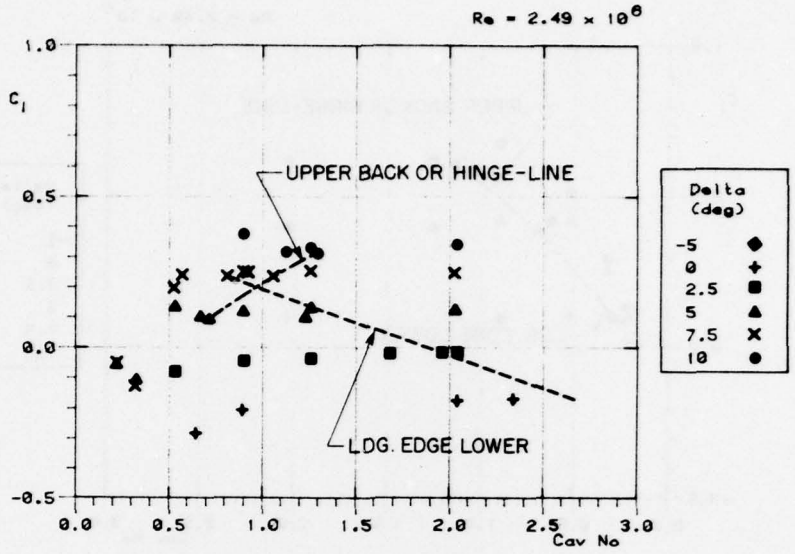


CL-VS-CAV NO AT -4 DEG ALPHA

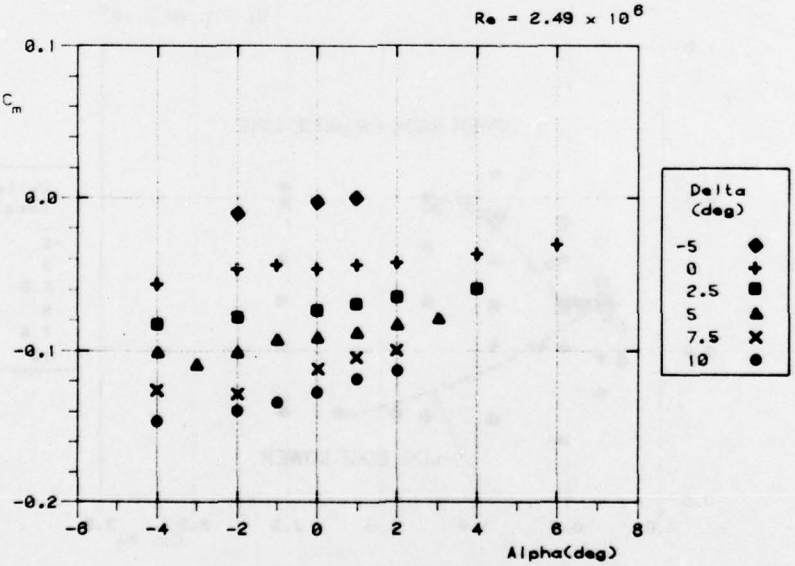


CM-VS-ALPHA FOR 2.04 CAVITATION NUMBER

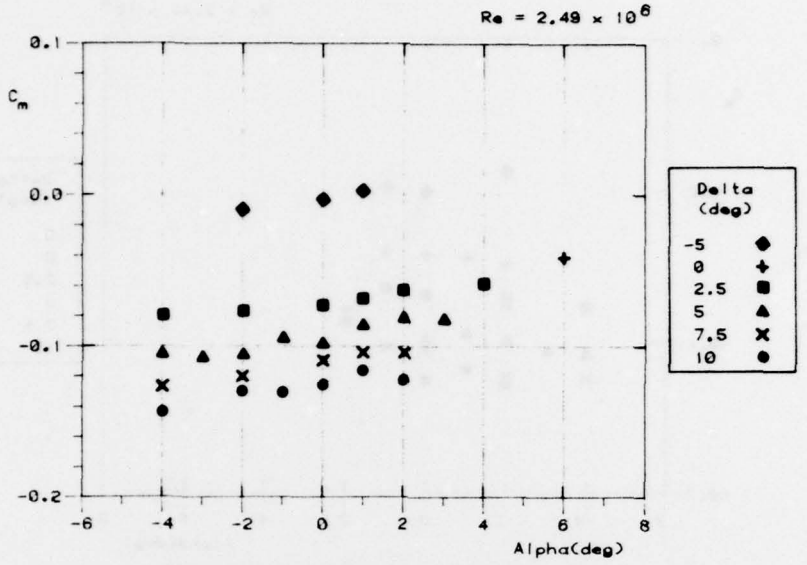


CM-VS-ALPHA FOR 1.26 CAVITATION NUMBER

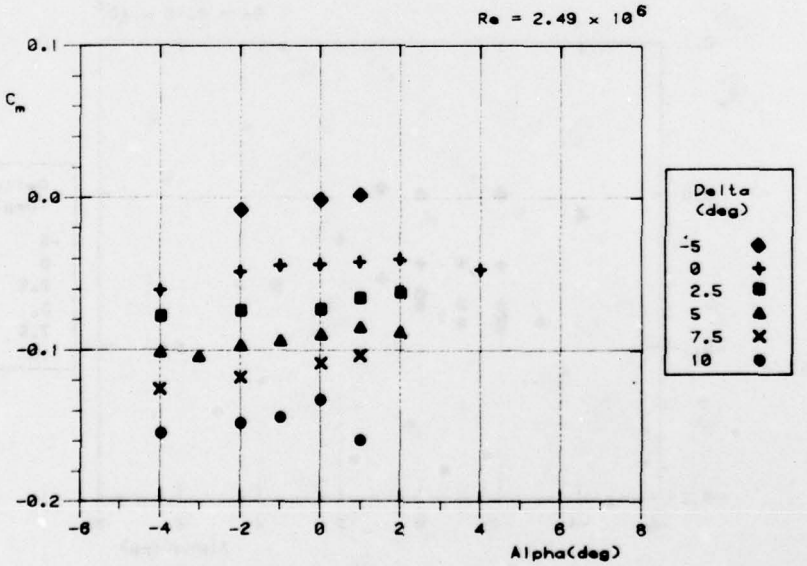


CM-VS-ALPHA FOR 0.90 CAVITATION NUMBER

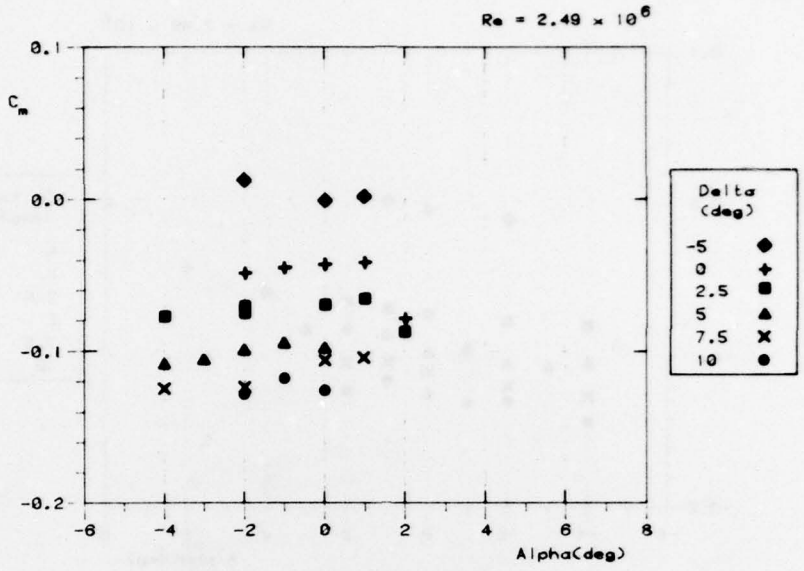


CM-VS-ALPHA FOR 0.53 CAVITATION NUMBER

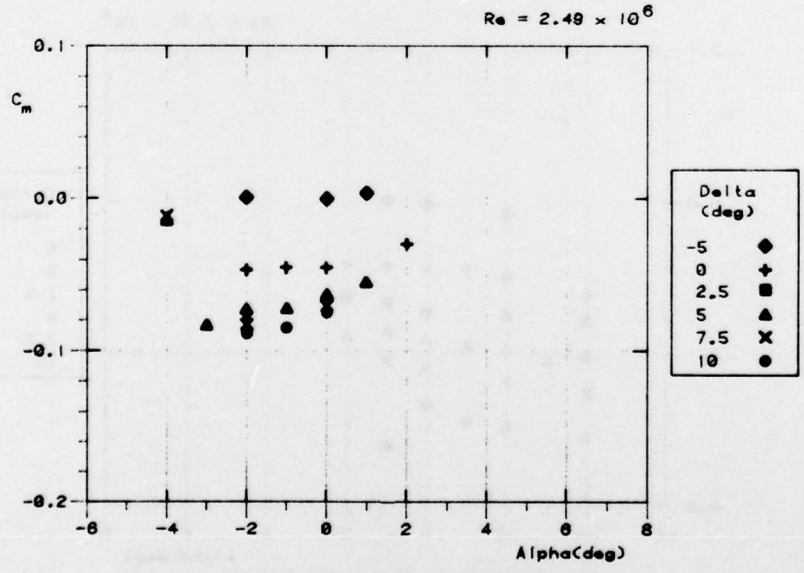


CM-VS-ALPHA FOR 0.33 CAVITATION NUMBER

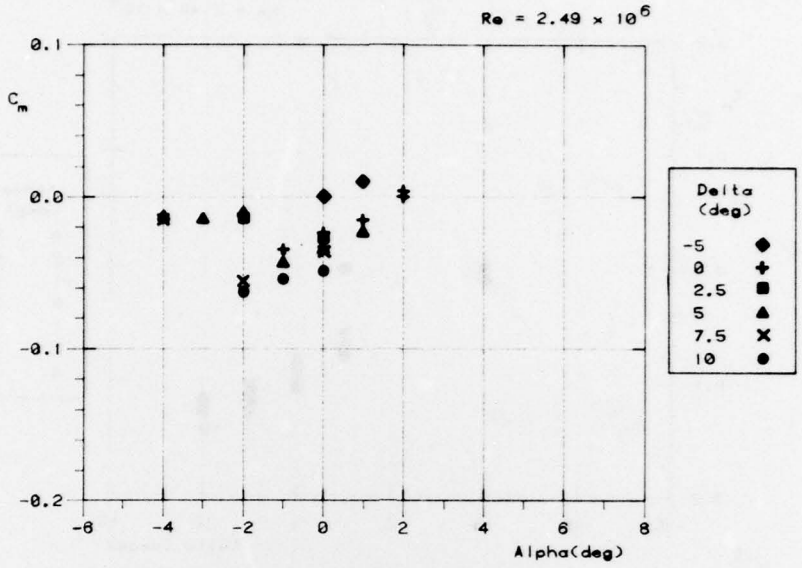


CM-VS-ALPHA FOR 0.22 CAVITATION NUMBER

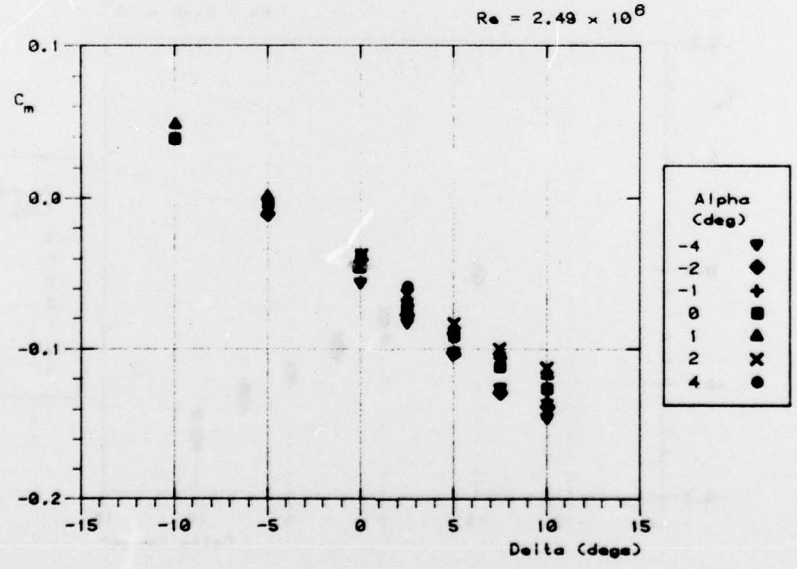


CM-VS-DELTA FOR 2.04 CAVITATION NUMBER

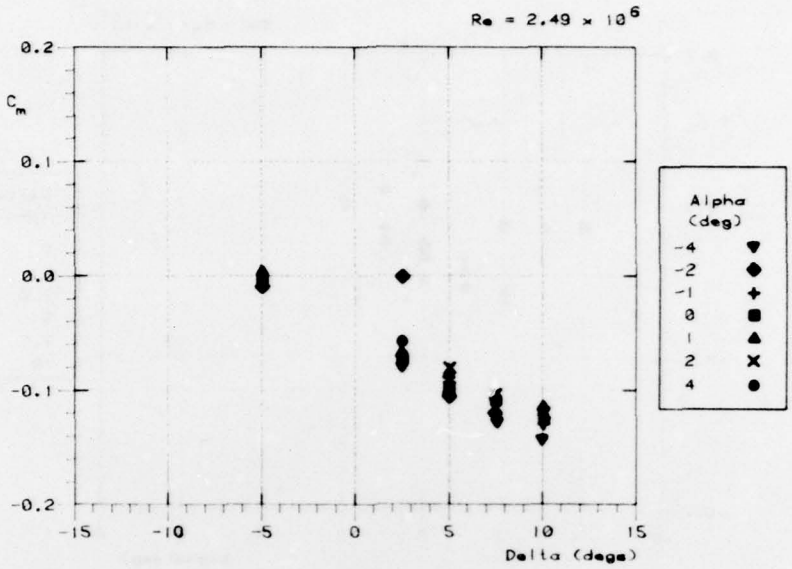


CM-VS-DELTA FOR 1.26 CAVITATION NUMBER

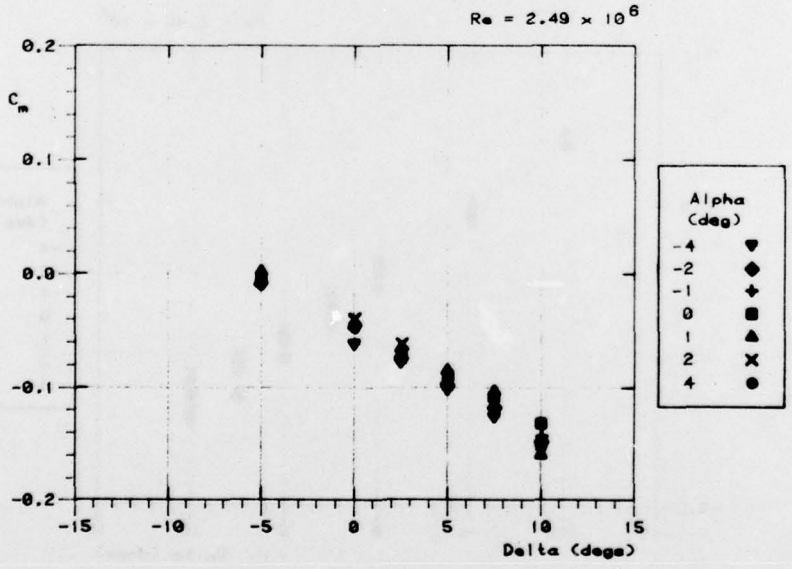


CM-VS-DELTA FOR 0.90 CAVITATION NUMBER

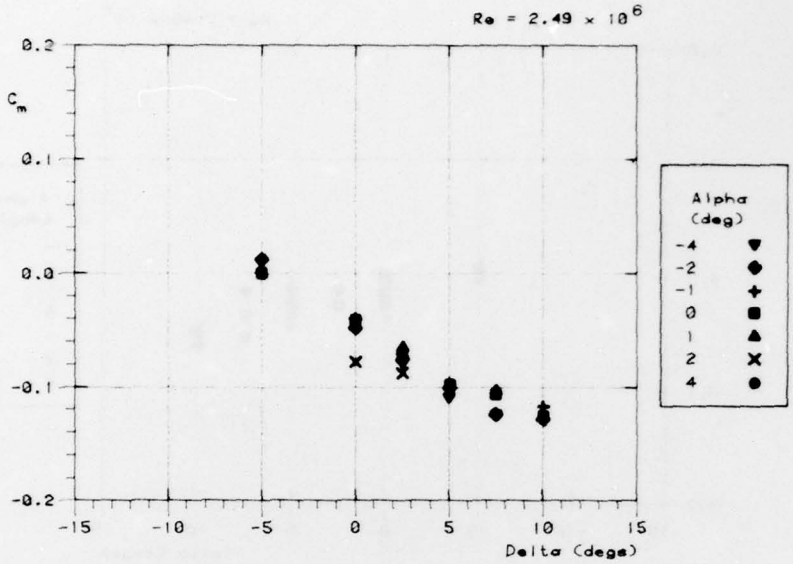


CM-VS-DELTA FOR 0.53 CAVITATION NUMBER

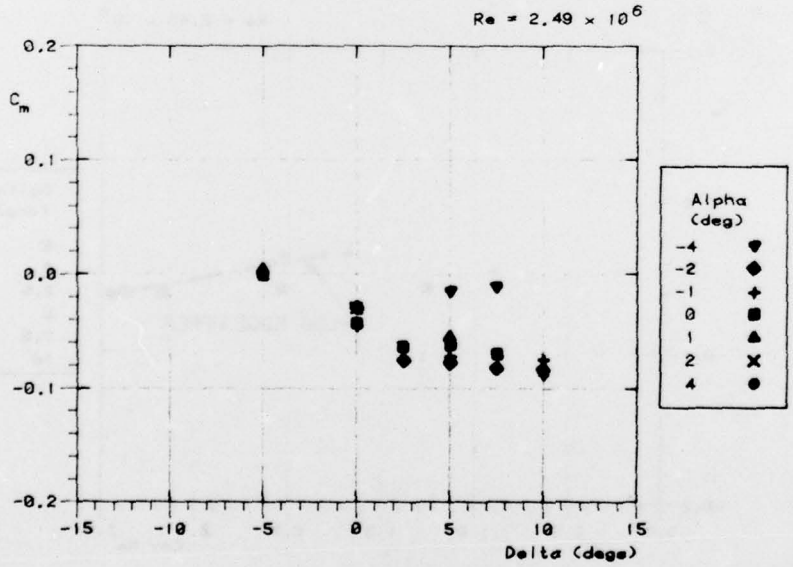


CM-VS-DELTA FOR 0.33 CAVITATION NUMBER

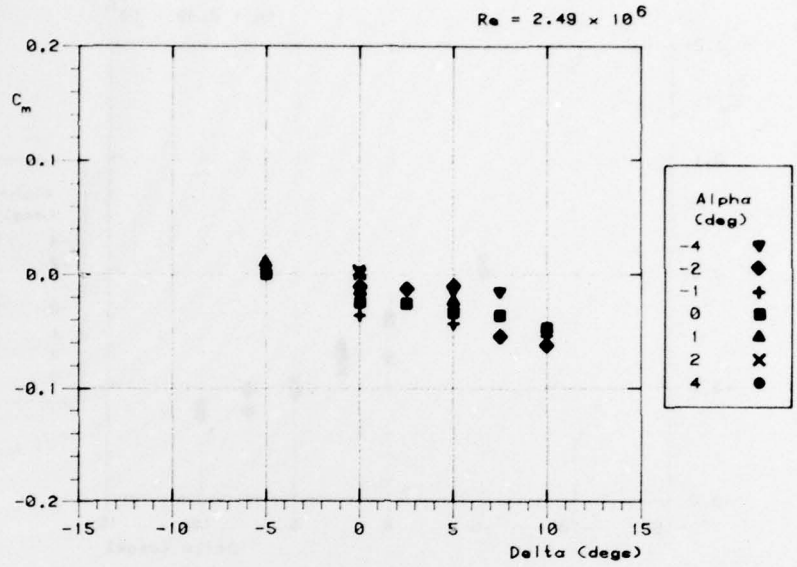


CM-VS-DELTA FOR 0.22 CAVITATION NUMBER

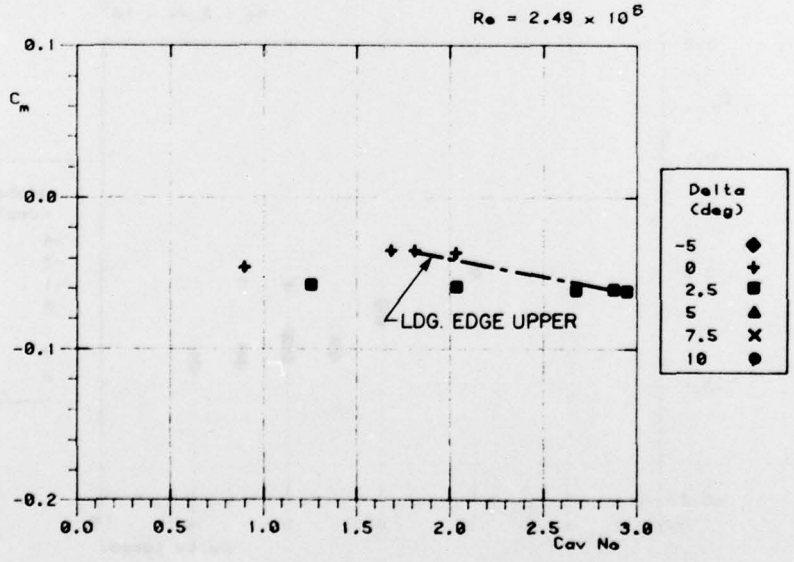


CM-VS-CAV NO AT 4 DEG ALPHA

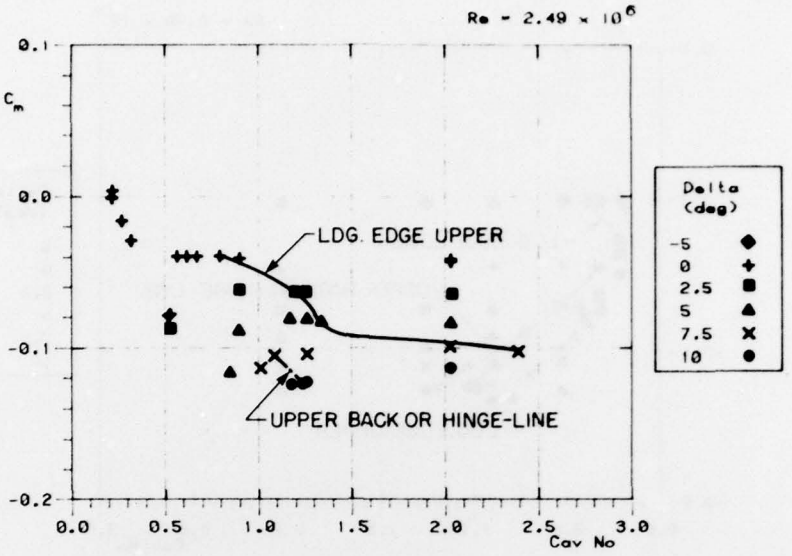


CM-VS-CAV NO AT 2 DEG ALPHA

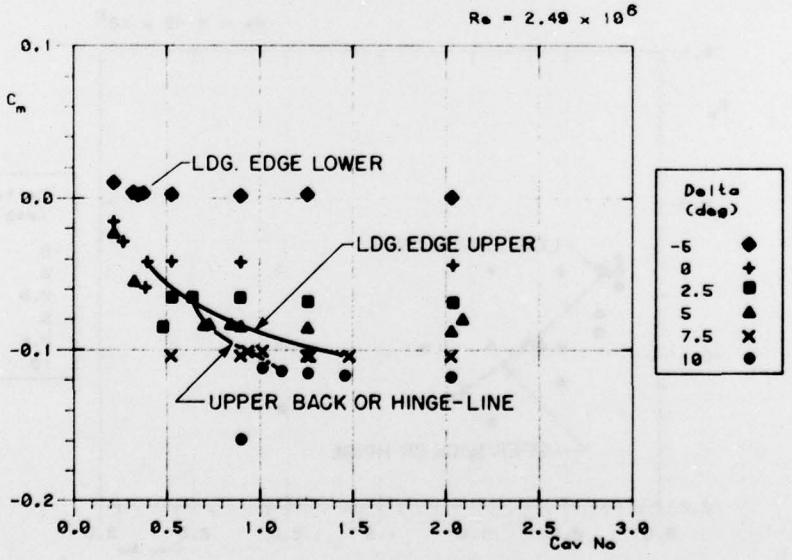


CM-VS-CAV NO AT 1 DEG ALPHA

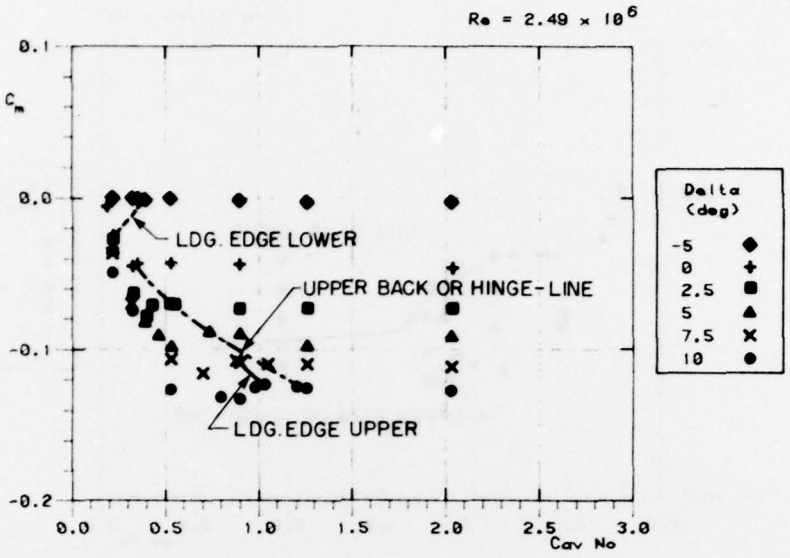


CM-VS-CAV NO AT 0 DEG ALPHA

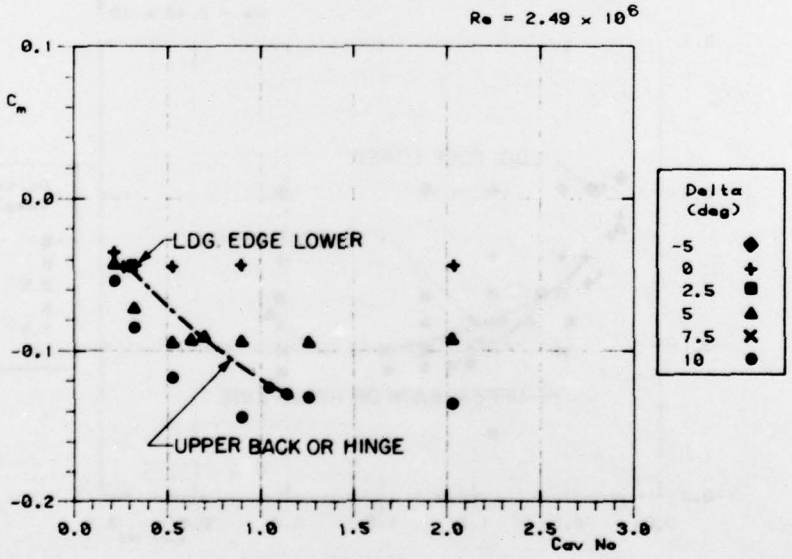


CM-VS-CAV NO AT -1 DEG ALPHA

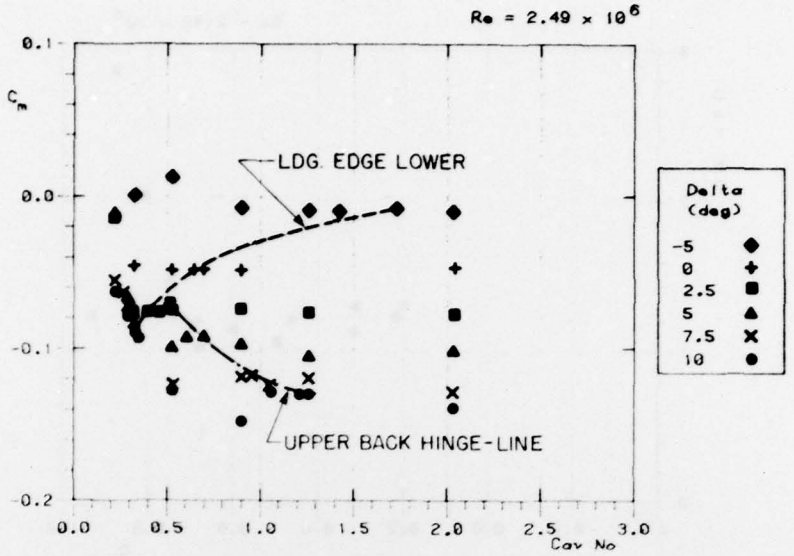


CM-VS-CAV NO AT -2 DEG ALPHA

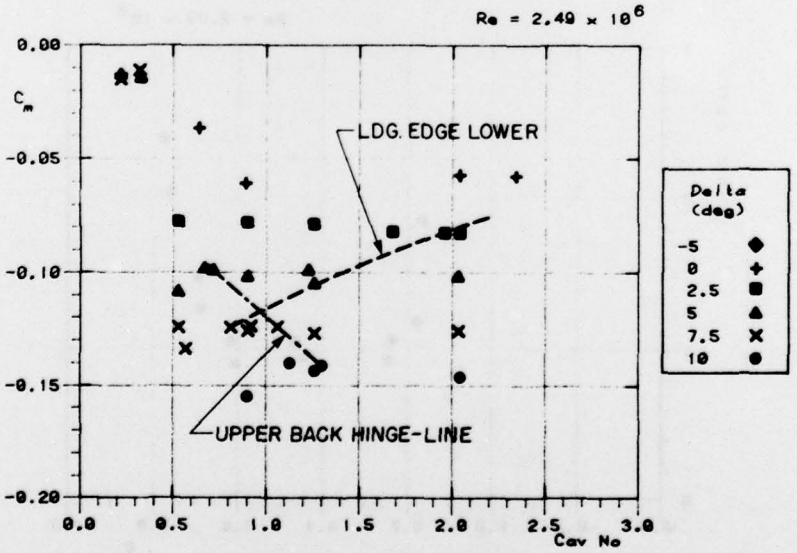


CM-VS-CAV NO AT -4 DEG ALPHA

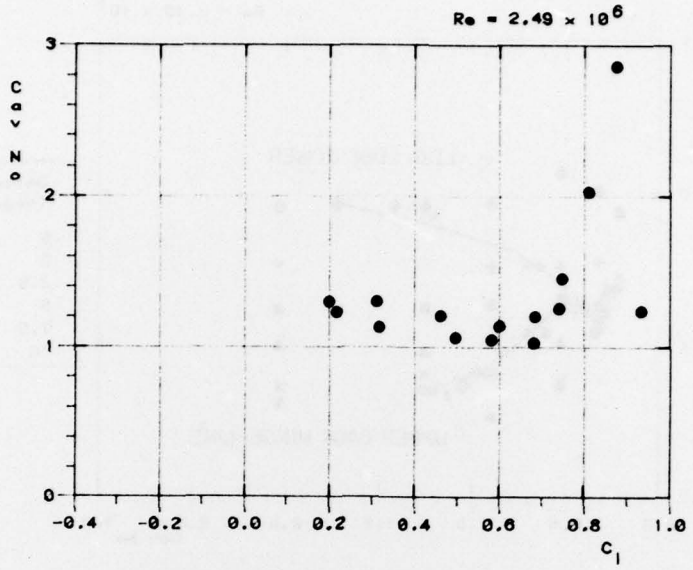


CAVITATION LIMIT DIAGRAM FOR 10 DEG DELTA

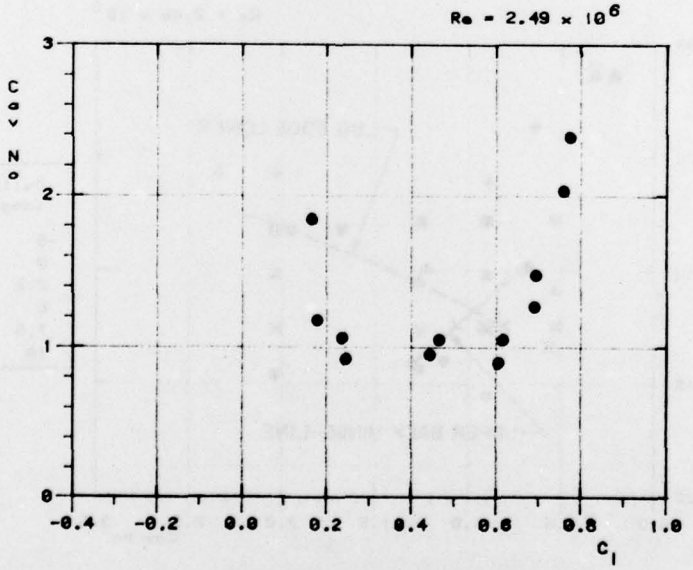


CAVITATION LIMIT DIAGRAM FOR 7.5 DEG DELTA

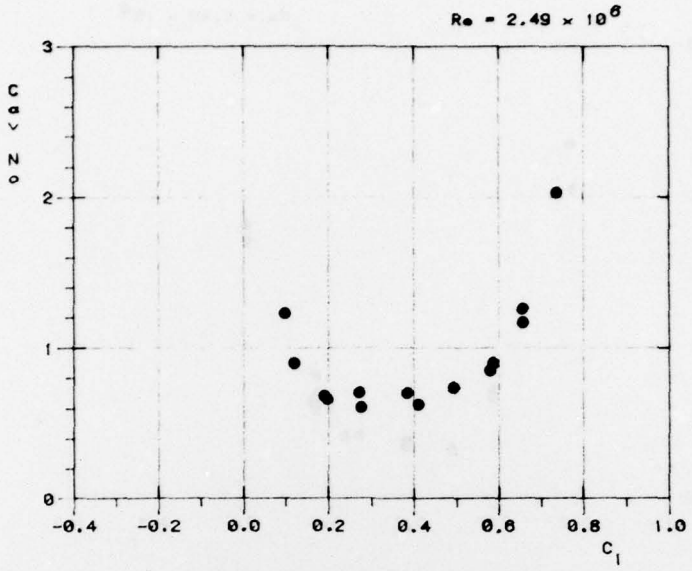


CAVITATION LIMIT DIAGRAM FOR 5 DEG DELTA

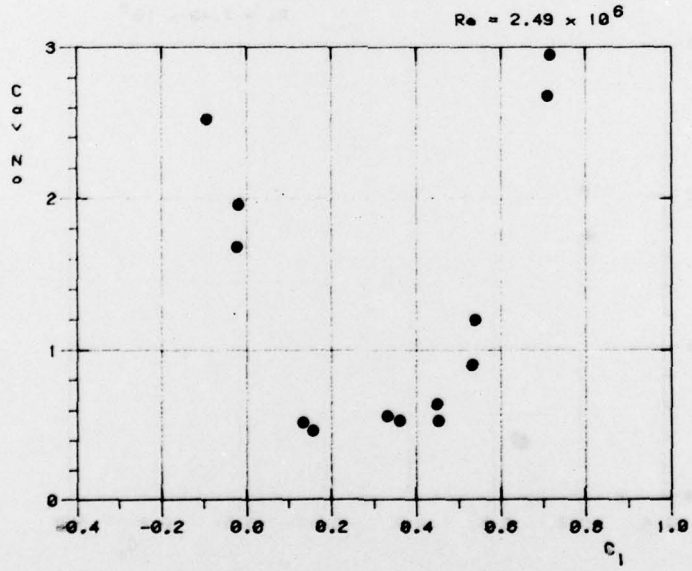


CAVITATION LIMIT DIAGRAM FOR 2.5 DEG DELTA

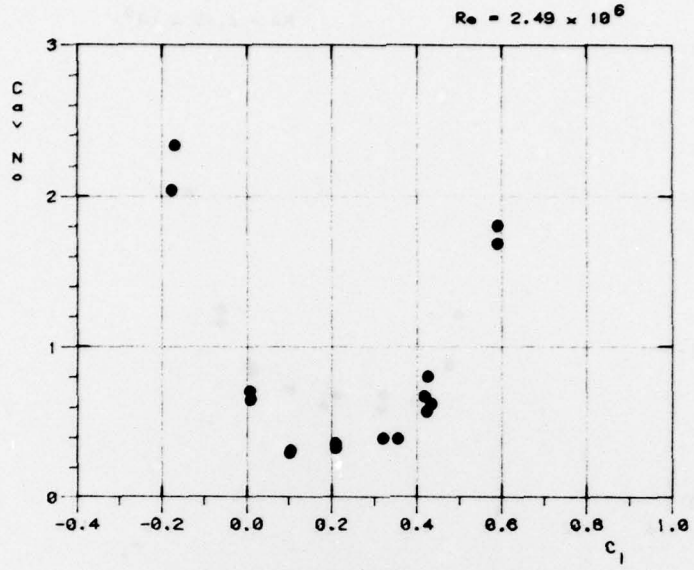


CAVITATION LIMIT DIAGRAM FOR 0 DEG DELTA

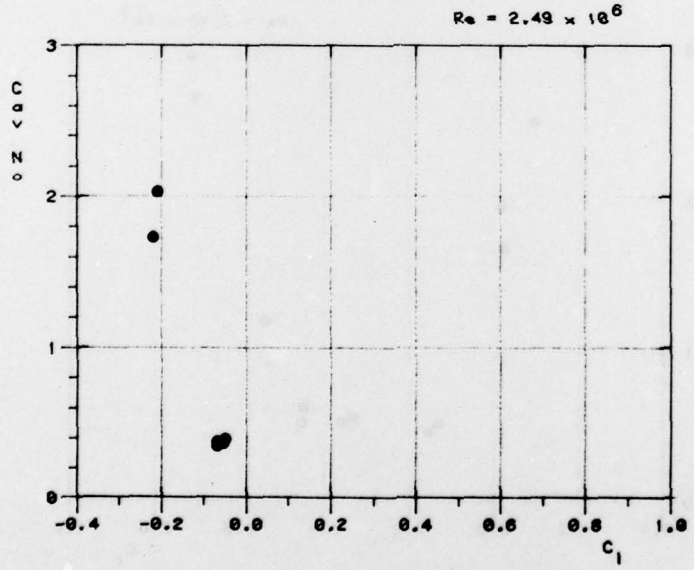


CAVITATION LIMIT DIAGRAM FOR -5 DEG DELTA

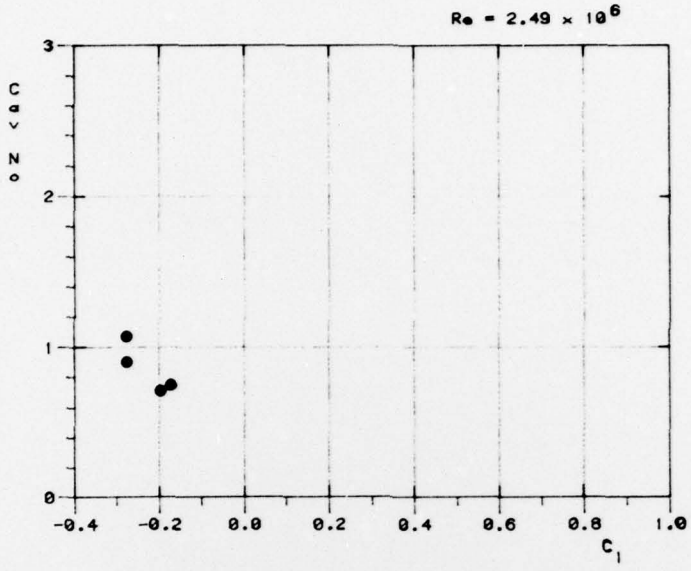


CAVITATION LIMIT DIAGRAM FOR -10 DEG DELTA

UNCLASSIFIED

Security Classification

**DOCUMENT CONTROL DATA - R & D**

(Security classification of title, body of abstract and indexing annotation must be entered when the overall document is classified)

| | |
|---|---|
| 1. ORIGINATING ACTIVITY<br>Defence Research Establishment Atlantic | 2a. DOCUMENT SECURITY CLASSIFICATION<br>UNCLASSIFIED<br>2b. GROUP |

3. DOCUMENT TITLE
"WATER TUNNEL TESTS ON A NACA 16-309 SECTION EQUIPPED WITH A SIMPLE, SEALED FLAP"

4. DESCRIPTIVE NOTES (Type of report and inclusive dates)
Technical Memorandum

5. AUTHOR(S) (Last name, first name, middle initial)
JONES, Eric A. and MACKAY, Michael

| | | |
|---|---|---|
| 6. DOCUMENT DATE | 7a. TOTAL NO. OF PAGES<br>63 | 7b. NO. OF REFS<br>9 |
| 8a. PROJECT OR GRANT NO.<br>23D | 9a. ORIGINATOR'S DOCUMENT NUMBER(S)<br>DREA Technical Memorandum 79/C | |
| 8b. CONTRACT NO. | 9b. OTHER DOCUMENT NO.(S) (Any other numbers that may be assigned this document) | |

10. DISTRIBUTION STATEMENT

| | |
|---|---|
| 11. SUPPLEMENTARY NOTES | 12. SPONSORING ACTIVITY<br>DREA |

13. ABSTRACT

Water tunnel tests are described of a NACA 16-309 section equipped with a 25% flap-chord ratio, simple, sealed flap. Lift and pitching moment coefficients are given for a range of angles of attack, flap angles and cavitation numbers. Drag data are not considered reliable and only a few values are presented. The results are also given of limited tests for the dependency of force, moment and cavitation inception data on Reynolds number over the range from 1.25 to 3.98 x $10^6$.

1,250,000 to 3,980,000

to the 6th power.

DSIS
79-070

**KEY WORDS**

NACA 16-309 section, flap, water-tunnel tests, wind-tunnel tests, cavitation, Reynolds number, boundary layer, separation.

**INSTRUCTIONS**

1. ORIGINATING ACTIVITY: Enter the name and address of the organization issuing the document.

2a. DOCUMENT SECURITY CLASSIFICATION: Enter the overall security classification of the document including special warning terms whenever applicable.

2b. GROUP: Enter security reclassification group number. The three groups are defined in Appendix 'M' of the DRB Security Regulations.

3. DOCUMENT TITLE: Enter the complete document title in all capital letters. Titles in all cases should be unclassified. If a sufficiently descriptive title cannot be selected without classification, show title classification with the usual one-capital-letter abbreviation in parentheses immediately following the title.

4. DESCRIPTIVE NOTES: Enter the category of document, e.g. technical report, technical note or technical letter. If appropriate, enter the type of document, e.g. interim, progress, summary, annual or final. Give the inclusive dates when a specific reporting period is covered.

5. AUTHOR(S): Enter the name(s) of author(s) as shown on or in the document. Enter last name, first name, middle initial. If military, show rank. The name of the principal author is an absolute minimum requirement.

6. DOCUMENT DATE: Enter the date (month, year) of Establishment approval for publication of the document.

7a. TOTAL NUMBER OF PAGES: The total page count should follow normal pagination procedures, i.e., enter the number of pages containing information.

7b. NUMBER OF REFERENCES: Enter the total number of references cited in the document.

8a. PROJECT OR GRANT NUMBER: If appropriate, enter the applicable research and development project or grant number under which the document was written.

8b. CONTRACT NUMBER: If appropriate, enter the applicable number under which the document was written.

9a. ORIGINATOR'S DOCUMENT NUMBER(S): Enter the official document number by which the document will be identified and controlled by the originating activity. This number must be unique to this document.

9b. OTHER DOCUMENT NUMBER(S): If the document has been assigned any other document numbers (either by the originator or by the sponsor), also enter this number(s).

10. DISTRIBUTION STATEMENT: Enter any limitations on further dissemination of the document, other than those imposed by security classification, using standard statements such as:

(1) "Qualified requesters may obtain copies of this document from their defence documentation center."

(2) "Announcement and dissemination of this document is not authorized without prior approval from originating activity."

11. SUPPLEMENTARY NOTES: Use for additional explanatory notes.

12. SPONSORING ACTIVITY: Enter the name of the departmental project office or laboratory sponsoring the research and development. Include address.

13. ABSTRACT: Enter an abstract giving a brief and factual summary of the document, even though it may also appear elsewhere in the body of the document itself. It is highly desirable that the abstract of classified documents be unclassified. Each paragraph of the abstract shall end with an indication of the security classification of the information in the paragraph (unless the document itself is unclassified) represented as (TS), (S), (C), (R), or (U).

The length of the abstract should be limited to 20 single-spaced standard typewritten lines; 7½ inches long.

14. KEY WORDS: Key words are technically meaningful terms or short phrases that characterize a document and could be helpful in cataloging the document. Key words should be selected so that no security classification is required. Identifiers, such as equipment model designation, trade name, military project code name, geographic location, may be used as key words but will be followed by an indication of technical context.